A signaling axis involving CNOT3, Aurora B and ERK promotes mesendodermal differentiation of ES cells

Moumita Sarkar[1,4]*, Matteo Martufi[1,4], Monica Roman-Trufero[1,4], Yi-Fang Wang[2], Chad Whilding[3], Dirk Dormann[3], Pierangela Sabbattini[1], Niall Dillon[1]*.

[1] Gene Regulation and Chromatin Group, [2] Bioinformatics and Computing, [3]Microscopy Facility, MRC London Institute of Medical Sciences, Hammersmith Hospital Campus, Du Cane Road, London W12 0NN, UK.

[4]These authors contributed equally to the study

*Correspondence to m.sarkar@lms.mrc.ac.uk, niall.dillon@lms.mrc.ac.uk

ABSTRACT

Mesendodermal cells are key intermediate progenitors that form at the early primitive streak (PrS) and give rise to mesoderm and endoderm in the gastrulating embryo. We have identified an interaction between CNOT3 and the cell cycle kinase Aurora B, requiring sequences in the NOT box domain of CNOT3, that regulates MAPK/ERK signalling during mesendodermal differentiation. Aurora B phosphorylates CNOT3 at two sites located close to a nuclear localization signal and promotes localization of CNOT3 to the nuclei of mouse ES cells (ESCs) and metastatic lung cancer cells. Mutating these sites in ESCs gives reduced numbers of embryoid bodies that are largely composed of ectoderm and interferes with differentiation of ESCs into mesendoderm in response to FGF2, BMP4, Wnt3 and Activin. The double mutation affects interaction of CNOT3 with Aurora B and ERK and reduces phosphorylation of ERK in response to FGF2. Our results identify an adaptor function for CNOT3 that regulates a key pathway in embryogenesis and cancer.

INTRODUCTION

A critical stage in mammalian embryogenesis is the formation of the ectoderm, mesoderm and endoderm germ layers that ultimately give rise to all of the somatic tissues in the embryo. Differentiation of the germ layers occurs during gastrulation, which begins at E6.5 in the mouse embryo with the formation of the primitive streak (PrS). The PrS starts as a region of mesendodermal (ME) differentiation that forms in response to localised signalling from the hypoblast/visceral endoderm (Stern and Downs, 2012). ME cells are transient precursor cells that differentiate from epiblast cells and express both mesodermal and endodermal markers (reviewed by (Wang and Chen, 2016). Ingression of these cells along the midline of the primitive streak is accompanied by differentiation into mesoderm and definitive endoderm and formation of the germ layers.

A number of signalling pathways and their associated ligands have been shown to be involved in specifying the location and timing of ME differentiation and primitive streak formation in the early embryo. The ligands that signal these events include Wnt3 (Tsakiridis et al., 2014) together with Activin, BMP4 and FGF2 (Ben-Haim et al., 2006; Bernardo et al., 2011; Fujiwara et al., 2002; Tremblay et al., 2000). Each of these ligands has different capacities for inducing differentiation of embryonic stem cells (ESCs) into mesoderm or endoderm. In combination they can be used to induce ESC differentiation of mesendoderm, which is characterised by expression of the mesodermal marker Brachury and endodermal markers GATA4, GATA6 and FOXA2. The fibroblast growth factor (FGF)/ ERK signaling pathway plays a vital role in the formation of mesendoderm in mouse and human ESCs (Wang and Chen, 2016; Yu et al., 2011).

The FGF/MEK/ERK signaling pathway functions in a large number of embryonic developmental processes, including proliferation, survival, migration, metabolism, and differentiation (Roskoski, 2012). Suppression of Erk signalling promotes ground state pluripotency in the mouse embryo and stimulation of ERK activity primes lineage commitment (Kunath et al., 2007; Nichols et al., 2009). The involvement of a single pathway in such a diverse range of outcomes implies the existence of multiple secondary levels of regulation that direct ERK/MAPK signals towards their different targets. Adaptor proteins that bind more than one signalling component are one type of mechanism that can be used to regulate ERK/MAPK activity and channel it towards specific specific targets in a given cell type (Kolch, 2005; Sacks, 2006).

CNOT3 was first identified as a component of the CCR4-Not complex, which is involved in regulating transcription and RNA processing in the nucleus and mRNA turnover in the cytoplasm (Collart, 2016). Studies in ESCs have shown that CNOT3 acts in conjunction with the transcription factors c-Myc and ZFX to form part of a transcriptional regulatory module, that binds to a number of gene promoters in ESCs (Hu et al., 2009) and has been reported to inhibit differentiation of ESCs into extraembryonic lineages (Hu et al., 2009; Zheng et al., 2012). Knockout of *Cnot3* in the mouse leads to embryonic lethality at the blastocyst stage caused by loss of inner cell mass cells (Neely et al., 2010). In addition to its early embryonic functions, CNOT3 has been shown to have important roles in B lymphopoesis (Yang et al., 2016) and maintenance of adipose tissues (Li et al., 2017) in adult mice. The *Cnot3* gene has also been shown to have tumour suppressor and tumour promoting properties (Cejas et al., 2017; De Keersmaecker et al., 2013; Shirai et al., 2019). Mutations that alter

the protein sequence have been identified in a range of cancers, with the largest number observed in prostate and colon cancers (Forbes et al., 2017; Priestley et al., 2019). The diverse biological and cellular roles of CNOT3 and the presence of a specialist protein-protein interaction domain, the NOT box, near the C-terminal of the protein suggest that it could function as an adaptor that mediates cross-talk between different cellular pathways.

Here we show that CNOT3 has the properties of an adaptor protein that links the cell cycle kinase Aurora B with the MAPK/ERK signalling pathway. Aurora B and ERK interact with the NOT box domain of CNOT3 and phosphorylation of the protein by Aurora B at sites adjacent to a nuclear localisation signal (NLS) promotes localisation of CNOT3 to the nucleus and increases interaction between ERK and CNOT3. Mutation of the Aurora B target sites reduces the level of active phosphorylated ERK in the nuclei of ESCs, preventing efficient differentiation of ME in response to FGF. We also present evidence supporting involvement of Aurora B-mediated phosphorylation and nuclear localisation of CNOT3 in the tumorigenic effects of CNOT3.

RESULTS

Phosphorylation by Aurora B localises CNOT3 to ESC nuclei.

The Aurora B cell cycle kinase phosphorylates multiple protein targets during mitosis and cytokinesis (reviewed in (Carmena et al., 2012)) and is also involved in regulating the G1 to S-phase transition (Song et al., 2007; Trakala et al., 2013). Upregulation of Aurora B protein levels has been shown to be a marker for lymph node metastasis in lung, colon and breast cancers (Takeshita et al., 2013; Tuncel et al., 2012; Zhang et al., 2015). We initially identified CNOT3

as a potential regulator of Aurora B in a co-immunoprecipitation screen and analysis that revealed a strong interaction between Aurora B and CNOT3 in primary resting and activated mouse B lymphocytes (Frangini, 2013), (M. Martufi and N. Dillon, unpublished data). Because of the known role of CNOT3 in pluripotency and lineage choice in ESCs, we tested whether it interacts with Aurora B in ESCs. Co-immunoprecipitation of ESC extracts with anti-Aurora B antibody showed that CNOT3 and Aurora B interact strongly in ESCs (Figure 1A).

Direct interaction of CNOT3 with Aurora B was demonstrated by *in vitro* pulldown with GST-tagged Aurora B, and the regions of CNOT3 that interact with Aurora B were identified by pulldown of *in vitro* translated ^{35}S-labelled CNOT3 mutant proteins that had specific regions of the protein deleted (Figure 1B, 1C, Figure S1A). The results of the deletion analysis showed that the C-terminal NOT box domain of the protein is essential for the interaction with Aurora B (Figure 1C, top panels). The analysis showed that deletion of the entire NOT box domain results in near-complete loss of Aurora B binding. Deletion of the N-terminal segment of the NOT box (650-700) had no effect on binding of Aurora B whereas deletion of the C-terminal region of the NOT box (700-750) strongly increased the amount of interaction observed. (Figure 1C, bottom panels). Deletion of the N-terminal region of CNOT3 (1-200) also reduced binding, although the reduction was less than the effect that was observed whe the NOT box domain was deleted. These results indicate a complex interaction between Aurora B and CNOT3, with binding dependent on the NOT box domain, but with other regions also contributing to binding, and different domains of the protein having both positive and negative effects on the interaction.

Inspection of publicly available high-throughput mass spectrometry data from human tissues (Hornbeck et al., 2015) revealed a phosphorylation hotspot extending from residues 291-299 of CNOT3 (Figure S1B). Mass spectrometry analysis of CNOT3 that was phosphorylated in vitro by Aurora B showed that phosphorylation occurs in vitro at residues T292 and S294 in the CNOT3 protein (Figure S2A). Examination of the CNOT3 sequence revealed that T292 is part of a consensus Aurora B phosphorylation site (^{290}R-S-T^{292}). Phosphorylation of purified *in vitro* translated wild-type and mutant CNOT3 proteins by Aurora B in the presence of [γ-^{32}P]-ATP showed reduced labelling of CNOT3 that had a double T292A/S294A mutation (Figure 1D). A reduction in labelling was also observed when T292 alone was mutated to A, but the effect was less pronounced when S294 was mutated on its own. Deletion of the NOT box region abolished labelling, indicating that docking of Aurora B on the NOT box is required for the kinase to efficiently phosphorylate CNOT3-T292/S294 (Figure 1D). It should be noted that mutation of T292/S294 does not completely eliminate in vitro phosphorylation implying that one or both of two Aurora B consensus sites in the protein amino-terminal and C-terminal regions of the protein (Figure S1A) are also targets for Aurora B when it binds to the NOT box.

The T292/S294 residues are located adjacent to a sequence motif (^{286}K-K-R-G-R^{290}) (Figure 1B, Figure S1A), which has been shown to form part of a functional nuclear localisation sequences (NLS) in the *Toxoplasma gondii* GCN5-B histone acetyl transferase and the Influenza D virus nucleoprotein(Dixon et al., 2011; Donchet et al., 2019; Tang et al., 2019). This led us to consider the possibility that phosphorylation by Aurora B might affect the nuclear localisation of CNOT3. To address this question, we first transfected V5-tagged CNOT3

expression constructs carrying mutations of either T292 or S294, or of both residues, to alanine, into HEK293 cells. The results showed reduction of nuclear CNOT3 for each of the single mutants and the double mutation, indicating that both sites contribute to nuclear localisation in this assay (Figure 1E).

In order to directly test the role of the two residues in regulating nuclear localization of endogenous CNOT3, the T292 and S294 residues were simultaneously mutated to alanine in mouse ESCs using CRISPR/Cas9 (Figure S2B). Generation of three ESC clones that were homozygous for the T292A/S294A double mutation was confirmed by sequencing (Figure S2B). The mutant ESCs grew normally and had the characteristic cell cycle profile of ESCs, although there was a small reduction in the proportion of S-phase cells compared with wild-type ESCs (Figure S2D and Figure S2E). Analysis of CNOT3 localisation by western blotting of nuclear and cytoplasmic fractions from wild-type (WT) and mutant (CNOT3-DM) ESCs showed a reduction in the amount of CNOT3 in the nuclei of mutant ESCs compared with WT cells (Figure 1E). Cytoplasmic levels of CNOT3 were largely unchanged in the mutant cells. These results provide strong evidence that phosphorylation of T292/S294 is involved in specifying localisation of CNOT3 to the ESC nucleus.

To determine whether the effect on nuclear localisation of CNOT3 is mediated by Aurora B, wild-type ESCs were incubated for 24 and 48 hours with the specific Aurora B inhibitor AZD1152. Comparison of the levels of CNOT3 in the nuclear and cytoplasmic fractions after 24 hours incubation with AZD1152 showed a substantial reduction in the amount of CNOT3 in the nucleus (Figure 1G) and the level was further reduced after 48 hours of treatment. The level of CNOT3 in the cytoplasm was largely unaffected (Figure 1G). Propidium iodide

staining and FACS analysis of the sorted cells showed only a minimal effect on the cell cycle with small increases observed in the numbers of G1 and G2 cells at both time points and and a small reduction in the number of S-phase cells at the 48 hour time point (Figure S2C and S2E).

Effect of mutating CNOT3-T292/S294 on embryoid body formation.

We set out to test whether the absence of phosphorylation of CNOT3-T292/S294 affected pluripotency and differentiation potential of the mutated ESCs. Wild-type and mutant ESCs were cultured under conditions that promoted the formation of embryoid bodies (EBs) (see Methods for details). EB formation was assessed after 4, 8 and 10 days of incubation under these conditions. The results show that the double *Cnot3* mutation (*Cnot3*-DM) resulted in a 40% reduction in EB numbers after 10 days in culture and the average size of the EBs was reduced by 40-50% (Figure 2A and 2B).

Staining of the EBs for the lineage markers Brachyury (mesoderm), FOXA2 (Endoderm) and Nestin (Ectoderm) revealed a striking difference between the wild-type and *Cnot3*-DM EBs (Figure 2C). The EBs formed from wild-type ESCs showed strong staining for all three markers, with Brachyury giving broad staining of the central and peripheral regions of the EBs, whereas FOXA2 staining was more restricted to the central regions. The ectodermal Nestin staining was broadly distributed in the EBs but was strongest at the periphery of the EBs. In contrast, the *Cnot3*-DM EBs showed very low staining for Brachyury or FOXA2 and strong central and peripheral taining for Nestin (Figure 2C). The pattern of ectodermal staining in the mutant EBs was confirmed by staining for the ectodermal marker OTX2 (Figure S3A). These results show that

the mutant EBs were predominantly composed of ectoderm, which suggests that blocking phosphorylation of CNOT3-T292/S294 interferes with germ layer formation.

CNOT3-T292/S294 phosphorylation promotes ME differentiation.

Formation of mesoderm and endoderm during gastrulation is thought to involve transtioning of cells through an intermediate ME stage at the PrS (Chuai et al., 2012; Costello et al., 2015; Wolfe and Downs, 2014). Nodal/Activin, Bmp, Wnt and FGF signaling pathways have been shown to have critical roles in ME differentiation (Bakre et al., 2007; Bertocchini and Stern, 2002; Tsakiridis et al., 2014; Vallier et al., 2009; Wang and Chen, 2016; Yu et al., 2011). To investigate the role of CNOT3-T292/S294 phosphorylation in ME formation, we carried out differentiations in a defined medium containing BMP4 and FGF2 and different combinations of Activin, Wnt and the GSK3β inhibitor CHIR99021, which stabilises β-catenin, bypassing Wnt activation (Alexanian et al., 2017) (Figure 3A-3C) (see Methods).

When applied to wild-type cells, all of the combinations that included BMP4 and FGF2 and either Wnt, Activin or CHIR99021 gave a high proportion of ME cells that stained for Brachyury and FOXA2 (Figure 3C). Incubation with FGF2 and BMP4 alone also promoted ME differentiation, but the number of differentiated cells was lower. Analysis of the mutant cells showed that differentiation in the presence of all ligand combinations tested gave significantly reduced numbers of differentiated cells (Figure 3B). The largest reductions in the number of mutant cells relative to wild-type were obtained with Wnt + FGF2 + BMP4 (80%) and FGF2 + BMP4 (65%).

The ability of the wild-type and *Cnot*3-DM cells to differentiate directly into mesoderm, endoderm and ectoderm was also tested (Figure S3C) (see Methods). Only in the case of differentiation into endoderm induced by FGF2 and retinoic acid, did we observe reduced differentiation of the mutant cells compared with the levels observed for wild-type cells (Figure S3C). These findings support the idea that the regulatory role of CNOT3-T292/S294 phosphorylation is linked to specific signalling pathways and suggest that FGF signalling is one of these pathways.

Survival of ME cells is enhanced by CNOT3 phosphorylation.

A more detailed characterisation of the effect of the *Cnot3*-T292A/S294A mutation on FGF2 and BMP4 signalling from day 2 to day 8 of ME differentiation showed reduced numbers of *Cnot3*-DM cells from day 2 onwards (Figure 4A, 4B). Staining for additional mesodermal and endodermal lineage markers (SMA: mesoderm; GATA4: endoderm) confirmed ME differentiation (Figure 4C and Figure S4A) The conclusion that proliferation and survival of ME cells is strongly affected by the double mutation was further reinforced by the results of a time-lapse analysis of the differentiating wild-type and mutant cells between 4 and 8 days of ME differentiation (Supplementary Video 1). The time-lapse analysis showed an explosive proliferation of the wild-type cells, whereas the *Cnot3*-DM cells failed to expand and appeared to undergo high rates of cell death following cell division. Analysis of the differentiation capacity of the other two *Cnot3*-T292A/S294A mutant clones that were generated by the CRISPR/CAS9 targeting showed a similar failure to expand and proliferate in the mesendoderm differentiation medium (Figure S4B), confirming that the effect was caused by

the double mutation. The cell cycle profiles of the wild-type and mutant cells after 4 days of differentiation were similar, implying that the major effect of the mutation was on survival of differentiating mesendoderm cells (Figure S4C).

The susceptibility of the *Cnot3*-DM cells to apoptosis during ME differentiation in response to FGF2 and BMP4 was directly assessed by staining wild-type and mutant cells with the apoptotic marker Annexin V and also by measuring propidium iodide (PI) uptake after 4 days of differentiation. The wild-type cells showed almost no staining for either cell death indicator whereas the 4-day differentiated mutant cells were strongly stained for PI and Annexin V, indicating that the failure of the mutant cells to differentiate was associated with high rates of apoptosis (Figure 4D). This result suggests a functional relationship between CNOT3 phosphorylation and survival signals mediated by incubation with FGF2 and BMP4.

The effect on survival of wild-type and mutant cells of either FGF2 + BMP4, activin only or Wnt only was directly compared (Figure S4D). The results showed that incubation with activin on its own gave reduced survival of wild-type cells compared with incubation of wild-type cells with FGF2 + BMP4 whereas survival of the mutant cells was similar under both conditions (Figure S4D). In contrast, cells that were incubated with Wnt in the absence of the other signalling ligands showed a reduction of around 10-fold in survival of wild-type cells and an even greater reduction for the *Cnot3*-DM cells (Figure S3B). These results highlight the importance of FGF2/BMP4 in promoting survival of the differentiating mesendoderm cells. In conjunction with the results in Figure 3B they also emphasise the strong synergy between Wnt and FGF2/BMP4 in promoting mesendoderm survival and differentiation, and they suggest that

phosphorylation of CNOT3-T292/S294 plays a role in the cross-talk between Wnt and FGF2/BMP4 signalling.

Gene expression analysis by RT-qPCR was used to measure mRNA levels for lineage markers in wild-type and mutant ME that was differentiated by treatment of FGF2/BMP4. The results from wild-type cells (Figure 5A) showed upregulation of mesodermal (*Brachury* and *MixL1*) and endodermal (*Gata4*, *Gata6*, *Sox17*, *Pdgfr*, *Cxcr4*) genes compared with undifferentiated ESCs, confirming that the cells were differentiating into ME. *Cdx2*, which is expressed in endoderm and trophectoderm, was also upregulated. However, expression of the early trophectoderm marker *Tead4* was very low in the differentiated cells (Figure 5A), indicating that the *Cnot3*-DM cells did not show a propensity to differentiate into trophectoderm under these conditions. Comparison of the *Cnot*-DM cells with wild-type cells showed that the mRNA and protein levels of ME genes were not significantly altered in the with the exception of *Brachury*, which showed reduced mRNA levels in the mutant cells (Figure 5B) and a smaller reduction at the protein level (Figure 5C). These results suggest that the major role of CNOT3 phosphorylation in ME differentiation is to promote survival of the differentiating cells.

These conclusions were reinforced by a transcriptomic comparison of the wild-type and *Cnot3*-DM cells using RNA-seq (Figure S5A and S5B). The RNA-seq analysis showed that 153 genes were significantly upregulated and 155 were downregulated in the mutant cells (Supplementary Tables 2A and 2B). Gene Ontology and GSEA analysis revealed that the mutation resulted in increased expression of genes that are associated with cell death and apoptosis (Figure S5C and S5E). In addition, genes involved in cell proliferation and the MAPK cascade

were downregulated (Figure S5D). The RNA-seq analysis also showed that the level of mRNA for FGFR1 which is the major FGFR that promotes ME differentiation (Ciruna and Rossant, 2001; Deng et al., 1994; Yamaguchi et al., 1994) was unchanged in the *Cnot3*-DM cells, whereas reduced expression was observed for FGFR2, which has an important role in trophectoderm differentiation (Xu et al., 1998).

Mutation of CNOT3-T292/S294 reduces ERK phosphorylation.

ERK1/2 signalling in response to stimulation by FGF is one of the major events that directs the transition from the pluripotent state to lineage commitment to the three germ layers and is critical for gastrulation (Kunath et al., 2007; Lanner and Rossant, 2010). FGFs acts through the FGF receptors (FGFRs) to activate the Ras/MEK/ERK pathway, which culminates in phosphorylation of MAPK/ERK at the threonine and tyrosine residues of the TEY motif (Roux and Blenis, 2004). Phospho-ERK is imported into the nucleus where it phosphorylates a number of transcription factors that are associated with proliferation as well as phosphorylating members of the RSK and MSK kinase families (reviewed in (Roux and Blenis, 2004)). There is also cross-talk between Wnt signalling and the Ras/MEK/ERK pathway, with Wnt signalling upregulating ERK phosphorylation by inhibiting GSK3β and preventing it from phosphorylating and destabilising Ras (Jeong et al., 2018; Wang et al., 2006). ERK has been reported to upregulate Aurora B expression in melanoma cells (Bonet et al., 2012) and phosphorylated ERK plays important roles in cell survival (Mebratu and Tesfaigzi, 2009).

Involvement of the FGF/MEK/ERK pathway in signalling cell survival during ME differentiation was supported by the observation that treatment of the cells with FGFR and MEK inhibitors caused a dramatic reduction in cell numbers (Figure 6A). This led us to consider the possibility of a functional interaction between Aurora B, CNOT3 and ERK that would cause the CNOT3 double mutation to affect ERK phosphorylation and cell survival. To assess the effect of the *Cnot3* T292A/S294A double mutation on ERK phosphorylation, extracts from wild-type and mutant ESCs that had been differentiated with FGF2 and BMP4 for 4 days were analysed by western blotting using an antibody that recognised the phosphorylated ERK TEY motif (Roux and Blenis, 2004) and an antibody against total ERK. The results showed a strong reduction in the level of phosphorylated ERK in the *Cnot3*-DM cells compared to wild-type (Figure 6B). Levels of phosphorylated ERK and ERK1/2 were unaffected in undifferentiated *Cnot3*-DM ESCs (Figure S6). Aurora B and CNOT3 continue to interact in differentiating ME cells, as shown by immunoprecipitations carried out with anti-CNOT3 antibody on extracts from the 4 day differentiated wild-type and Cnot3-DM cells (Figure 6C). Levels of total CNOT3 were reduced in differentiated *Cnot3*-DM cells (Figure 6B), suggesting that phosphorylation by Aurora B stabilises wild-type CNOT3, similar to the effect that has been reported for Aurora B and Aurora C phosphorylation of INCENP (Sasai et al., 2016).

Altered interaction of mutant CNOT3 with Aurora B and ERK.

To analyse interactions between CNOT3, Aurora B and ERK at the single-cell level during ME differentiation, we made use of the proximity ligation assay (PLA). ESCs were incubated for 4 days in differentiation medium containing

FGF2 and BMP4 and then subjected to PLA using mouse anti-Aurora B and rabbit anti-CNOT3 antibodies. (see Methods). The results of this analysis showed a high level of association between CNOT3 and Aurora B in wild-type cells after 4 days of differentiation (Figures 7A). The number of interaction foci in the nuclei of wild-type cells was around half the number observed in the cytoplasm.

Analysis of the *Cnot3*-DM cells showed an unexpected increase of approximately 3-fold in the interaction between CNOT3 and Aurora B in the mutant cells compared to the wild-type cells after 4 days of ME differentiation (Figure 7A). The increased signal was accompanied by an increase in the proportion of interaction foci observed in the nucleus relative to the cytoplasm compared to wild type cells. Overall, these results confirm the strong interaction between CNOT3 and Aurora B that was observed by co-IP of extracts from undifferentiated ESCs and after 4 days of ME differentiation. The differences between the interaction patterns observed in the wild-type and Cnot3-T292A/S294A mutant cells suggest that phosphorylation of T292/S294 by Aurora B plays an important role in regulating the dynamic behaviour of CNOT3 in differentiating ME cells.

PLA of the interaction between CNOT3 and ERK showed a substantial level of interaction in wild-type 4-day differentiated cells that was broadly distributed between cytoplasmic and nuclear compartments. The mutant cells showed significant reductions in both compartments, with the cytoplasm showing a 3-fold reduction and the nuclei a 5-fold reduction in the number of interaction foci observed (Figure 7B). These results, which were confirmed with a second, separate anti-CNOT3/anti-ERK antibody pair (Figure S7A, S7B), provide strong evidence that ERK interacts with CNOT3 and that this interaction

is promoted by Aurora B-mediated phosphorylation of CNOT3-T292/S294. The observation that mutation of the Aurora B phosphorylation sites reduces phosphorylation of ERK suggests that the interaction between ERK and phosphorylated CNOT3 promotes or stabilises ERK phosphorylation, thereby enhancing Ras/MEK/ERK signalling.

In vitro pulldown of GST-ERK with ^{35}S-labelled CNOT3 showed that ERK interacts directly with Aurora B (Figure 7C). Analysis of CNOT3 deletion mutants showed some similarities to the binding of Aurora B, with deletion of the NOT box abolishing binding and deletion of the C-terminal region enhancing the interaction with GST-ERK. However, the effects of the CNOT3 deletions showed some differences from the effects that we observed on Aurora B binding (Figure 1C), with the the Δ651-700 deletion mutant showing a 50% redunction in ERK binding whereas the same mutation did not give a reduction in binding of Aurora B. This implies that there are differences in the contacts that Aurora B and ERK make with the CNOT3 NOT box region.

Phosphorylation alters localisation of CNOT3 in cancer cells.

Mutations in the coding region of human *Cnot3* have been observed in a number of cancers (Forbes et al., 2017), with genetic analysis providing evidence that *Cnot3* mutations can have tumour suppressor (De Keersmaecker et al., 2013) and tumour promoting (Delacruz et al., 2019) effects. High levels of nuclear CNOT3 have also been observed in an aggressive colorectal cancer cell line (Cejas et al., 2017). These observations, together with our results, led us to consider the possibility that Aurora B might be promoting nuclear localisation and EMT/MET in cancer cells. To test this hypothesis, H1299 and A549 non-

small cell lung cancer (NSCLC) cells were stained with anti-CNOT3 antibody. H1299 was originally derived from a lymph node metastasis and A549 from a lung adenocarcinoma. The results of the immunofluorescence analysis (Figure 8A) showed that nuclear CNOT3 levels were approximately 3-fold higher than the cytoplasmic levels in H1299 cells, whereas the difference was 1.6-fold in A549 cells.

Involvement of Aurora B phosphorylation in the H1299-specific localisation of CNOT3 was investigated by treating H1299 cells for 3 hours with AZD1152. The incubation time was optimised to avoid disruption of the cell cycle. The results show a dramatic effect of Aurora B inhibition on CNOT3 localisation in the H1299 cells with the nuclear levels of CNOT3 in the inhibitor-treated cells reduced by 3-fold relative to the cytoplasmic level (Figure 8B).

The involvement of the NLS and the Aurora B target sites in cancer is further supported by the recent identification of a *Cnot3*-K286E mutation in 11% (4/37) of a cohort of pre-malignant adenomas from that were sequenced from Familial Adenomatous Polyposis (FAP) patients (Delacruz et al., 2019) (Figure 8C). *Cnot3*-K286 is the first residue of the KKRGR nuclear localisation sequence that is located adjacent to the sites of Aurora B phosphorylation in mouse ESCs. Mutations that affect the first residue of the Aurora B consensus (*Cnot3*-R290C and -R290H) have also been described in one lung and three colorectal cancers (Forbes et al., 2017; Giannakis et al., 2016; Priestley et al., 2019). Overall, a total of nine cancer patients have been shown to have mutations in the NLS (Figure 8C). This clustering of mutations provides strong evidence of a role for this region in oncogenic progression, particularly in colorectal cancers. The R286E, R290H and R290C mutations would be expected to reduce nuclear uptake of

CNOT3 in response to Aurora B, leading to downregulation of ERK phosphorylation. This is consistent with reports that ERK, in addition to its tumour promoting properties, can also act as a tumour suppressor by potentiating oncogene-induced sensescence (Deschenes-Simard et al., 2013). Another possibility is that the region containing the NLS and Aurora B target residues also interacts with other as yet identified proteins that have tumour promoting or suppressive effects.

DISCUSSION

The epithelial to mesenchymal transition (EMT) that leads to mesendodermal differentiation and gastrulation is a critical stage in mammalian embryogenesis. Our results identify a role for CNOT3 in regulating the signalling pathways that promote mesendodermal differentiation in the early embryo. The effect occurs through direct interaction between CNOT3 and the Aurora B kinase, with Aurora B-mediated phosphorylation of specific sites adjacent to an NLS within the CNOT3 protein resulting in increased localization of CNOT3 to the nucleus. The interaction between Aurora B and CNOT3 is completely dependent on the NOT box domain of CNOT3. An additional weaker requirement for the N-terminal region of the protein suggests that there is synergistic binding of Aurora B to these two regions. When the NLS-adjacent Aurora B phosphorylation sites in the CNOT3 protein were mutated in ESCs, embryoid bodies formed from the mutant cells showed a dramatic reduction in differentiation of mesoderm and endoderm, with the mutant EBs being largely made up of ectoderm.

Differentiation of the *Cnot3*-T292A/S294A mutant ESCs into mesendoderm in response to different combinations of Activin, Wnt, BMP4 and

FGF2 showed that the capacity of all four ligands to induce mesendoderm was affected by mutation of the Aurora B sites in CNOT3. The largest effect of the mutation on differentiation was observed for the combination of Wnt, BMP4 and FGF2. This suggests involmement of CNOT3 in the cross-talk that is known to occur between Wnt signalling and the RAS/MEK/ERK pathway (Georgopoulos et al., 2014; Jeong et al., 2018).

The observation that CNOT3 mutant cells induced to differentiate with FGF2 and BMP4 showed evidence of apoptosis whereas wild-type cells did not, suggested that CNOT3 is involved in pathways that regulate survival of differentiating mesendoderm cells, with activation of ERK signalling in response to FGF2 being a major candidate. This was supported by the observation that the numbers of differentiated cells obtained with wild-type cells were strongly affected by inhibition of FGF2. Analysis of ERK phosphorylation showed that ERK activation is indeed affected by the *Cnot3* double mutation with a strong reduction in the levels of phosphorylated ERK observed in the mutant cells. This finding provides a direct mechanistic explanation for the increased apoptosis observed in the *Cnot3*-DM cells when differentiation is induced using FGF2 and BMP4.

How might the level of phosphorylated ERK be increased by Aurora B-mediated phosphorylation of CNOT3? Phosphorylation of ERK by MEK is followed by rapid import of phospho-ERK into the nucleus, which occurs through a variety of mechanisms (Mebratu and Tesfaigzi, 2009). Phospho-ERK is also subject to dephosphorylation in the nucleus and to re-export to the cytoplasm. The level of phospho-ERK in the nuclear compartment is known to be strongly dependent on binding of ERK to stabilising proteins in the cytoplasm and in the

nucleus (Caunt and McArdle, 2012; Mebratu and Tesfaigzi, 2009; Pouysségur and Lenormand, 2003) The results of the *in vitro* GST pulldown and *in vivo* PLA analyses indicate that ERK interacts with CNOT3 via the NOT box domain in differentiating mesendodermal cells and that this interaction is reduced in the Cnot3-DM mutant cells by 3-fold in the cytoplasm and by 5-fold in the nucleus. The observation that the double mutation increases interaction with Aurora B and reduces the CNOT3-ERK interaction, suggests a model (illustrated schematically in Figure 9) where the two kinases interact sequentially with CNOT3, with Aurora B first interacting with the CNOT3 NOT-box, followed by phosphorylation of CNOT3 at the NLS and release of the bound Aurora B allowing ERK to bind to the NOT box. Our finding that Aurora B phosphorylation promotes localization of CNOT3 to the nucleus also suggests that the interaction between phosphorylated CNOT3 and ERK could be involved in stabilising phospho-ERK in the cytoplasmic and nuclear compartments and potentially in the transport of phospho-ERK into the nucleus.

In addition to these conclusions, the increased nuclear localisation of CNOT3 that we observe in an NSCLC cell line that was isolated from a lymph node metastasis opens up the possibility that nuclear localisation of CNOT3 promotes EMT/MET in cancer cells, acting as a driver for metastasis.. The known association of elevated Aurora B levels with lymph node metastasis in a number of cancers (Takeshita et al., 2013; Tuncel et al., 2012; Zhang et al., 2015) and the well established involvement of MAPK/ERK pathways in tumourigenesis and metastasis (Bang et al., 1998; Sebolt-Leopold et al., 1999; Smith et al., 2014) suggests that the interaction of CNOT3, Aurora B and ERK has important roles in the development and progression of human cancers.

Overall, our results provide evidence of a signaling axis between ERK and Aurora B with CNOT3 acting as an adaptor that links the the two kinases. Our findings suggest that Aurora B acts through CNOT3 to increase the level of phospho-ERK, thereby promoting survival and differentiation of ME cells. These observations indicate that the synergy between the three proteins plays an important role in regulating EMT during ME differentiation and gastrulation of the mouse embryo. The very strong reduction in survival and proliferation that we observe when the *Cnot3*-DM cells are induced to differentiate into ME suggests that Aurora B links up with the MAPK/ERK and Wnt pathways via CNOT3 to promote the explosive expansion of cell numbers that occurs in the embryo at the time of implantation and gastrulation.

MATERIALS AND METHODS

Cell Culture

E14 ESCs (female, 129/Ola) were obtained from the LMS Transgenics and ES cell facility. The ESCs were maintained on gelatin coated plates, at 37°C, 5% CO_2, in KnockOut Dulbecco's Modified Eagle's Medium supplemented with 15% fetal bovine serum, 1x NEAA, 2 mM L-glutamine, 100 units/ml penicillin, 100 μg/ml streptomycin, 100 μM βME (all reagents from Thermo Fisher Scientic) and 1000 units/ml LIF (Merck). HEK 293 cells and A549 cells(ATCC) were maintained in Dulbecco's Modified Eagle's Medium supplemented with 10% fetal bovine serum, 2 mM L-glutamine, 100 units/ml penicillin and 100 μg/ml streptomycin. H1299 cells (ATCC) were maintained in RPMI-1640 media supplemented with the same condstituents as mentioned above.

CNOT3 gene editing using CRISPR/Cas9

The guide RNA (gRNA) used to generate the *Cnot3*-T292A/S294A mutant ESCs was 5'-GATTTAGACTTGGACCCACC-3'. The gRNA was cloned into pX330 (Addgene plasmid #42230) using forward primer 5'-CACCGGATTTAGACTTGGACCCACC-3' and reverse primer 5'-AAACGGTGGGTCCAAGTCTAAATCC-3'

The 110 base paired single stranded donor DNA used to target *Cnot3* in exon 10 carrying the mutations was: 5'-ACTCTGAAGATGATAAGAAGAGAGGCCGATCTGCGGATGCTGAAGTCAGCCAGGTGGGTCCAAGTCTAAATCTGATGGTTTGTAACTTGTTTATTGCGTGGTCTCCAAAG-3'

Mouse ESCs ($4x10^6$ cells) were transfected with 3 μg of pX330 plasmid carrying the gRNA, 4 μg of the donor ssDNA and 3 μg of a puromycin resistance plasmid (pCAG-puro^R) using the Mouse ES Cell Nucleofector™ Kit (Lonza) following the manufacturer's protocol. One day post transfection cells were subjected to puromycin selection (1.5 μg/ml) for 24 hours. A week after transfection, individual clones were picked and genotyped by allele specific nested PCR. Mutant genotypes were confirmed by sequencing.

Embryoid bodies

Half a million cells (per well of a six well plate) were seeded on ultra-low attachment plates (Corning Costar) and maintained in KnockOut Dulbecco's Modified Eagle's Medium supplemented with 15% fetal bovine serum, 1x NEAA, 2 mM L-glutamine, 100 units/ml penicillin, 100 μg/ml streptomycin, 100 μM βME and were grown up to 14 days.

Embryoid bodies (EBs) were fixed in 4% paraformaldehyde for twenty minutes followed by permeabilization with 0.5% Triton-X for twenty minutes. Subsequently, EBs were blocked in 3% BSA for one hour and then incubated

with primary antibodies overnight at 4°C. On the following day, the EBs were washed 3 times with PBS+0.1 % Tween-20 (PBST) and incubated for 1hour at room temperature with the appropriate secondary antibodies. Embryoid bodies were then washed three times in PBST and incubated with 1μg/ml DAPI in PBS for 45 minutes. Images were acquired using a Leica SP5 confocal microscope (objective x10) with LAS X software (Leica) and images were analysed with Fiji ImageJ software.

Differentiation experiments

ESC differentiation into mesendoderm: Cells were plated at a density of 10000 cells/cm^2 on gelatin-coated plates and incubated in DMEM/F12 KnockOut media containing 64 μg/ml of L Ascorbic acid-2-phosphate magnesium, 543 μg/ml of sodium bicarbonate, 1 μg/ml of heparin, 1x insulin-transferrin-selenium and 2mM Glutamine. For the differentiations, different combinations of signalling factors were added to the medium (see "Treatments of the cells with ligands and inhibitors" below). For time-lapse imaging of differentiation from day 3 to day 7, the plate was transferred to a Zeiss Axiovert 200 microscope with environmental chamber (Solent Scientific Ltd.) and motorised stage (ASI) and images were collected at an interval of thirty minutes. Phase contrast images were acquired in Leica DMIRE2 microscope using the MetaMorph software.

ESC differentiation to endoderm: Cells were plated at a density of 10000 cells/cm^2 on gelatin-coated plates and incubated in high glucose DMEM with 15% FBS, 100 units/ml penicillin, 100 μg/ml streptomycin, 0.1 mM non-essential amino acids, 1mM MTG, 1x GlutaMAX and supplemented with 25 ng/ml of FGF2 (Merck) and 10 μM of retinoic acid (Merck)for 3 days (Kim et al., 2010).

ESC differentiation to mesoderm: Cells were plated at a density of 15000 cells/cm^2 in gelatin + fibronectin-coated plates and incubated for 4 days in DMEM/F12-Neurobasal (1:1), N2, B27, 1x GlutaMAX, 100 units/ml penicillin, 100 μg/ml streptomycin, 0.1% β-ME and 30 ng/ml of Activin A (R&D Systems).

ESC differentiation to ectoderm: Cells were plated at a density of 15000 cells/cm^2 on gelatin-coated plates and incubated for 4 days in DMEM/F12-Neurobasal medium (1:1), 1x GlutaMAX, 100 units/ml penicillin, 100 μg/ml streptomycin, 100 μM βME, B27 minus Vitamin A and N2.

Treatment of cells with ligands and inhibitors

Aurora B inhibitor AZD1152 (Merck)-200 nM; human recombinant Wnt3 (Cloud-Clone Corp)-200 ng/ml; Activin A (R&D Systems)-100 ng/ml; BMP4 (Merck)-10 ng/ml; FGF2 (Merck)- 25ng/ml; CHIR99021(Merck)-3μM, PD0325901 (Merck)-500nM; U0126(Merck)-10μM; AZD4547 (Abcam)-5nM.

Cell survival assay and Annexin V staining

The Annexin V staining was performed using the FITC Annexin V apoptosis detection kit with PI (BioLegend). The cells were washed with PBS followed by washing with staining buffer and resuspension in binding buffer containing anti-Annexin V and PI and incubation for fifteen minutes at room temperature in the dark. The cells were finally washed with binding buffer and incubated with 1μg/ml DAPI in PBS for 5 minutes. Images were acquired using an Olympus IX70 microscope with Micro-manager software.

Cells were stained with 0.2% crystal violet for a gross estimation of efficiency of differentiation. At different time points of differentiation live and dead cells were distinguished by trypan blue staining and counted manually. Cell survival was measured using Cell Proliferation Reagent WST-1 (Merck) at a final dilution of

1:10 followed by incubation for half an hour and quantitation with a scanning multi-well spectrophotometer (SpectraMax-Molecular Devices).

Immunocytochemistry

All differentiated cells were grown in gelatin coated μ-slides (ibidi) for immunofluorescence. Cells were washed in PBS and fixed in 4% paraformaldehyde for ten minutes followed by permeabilization with 0.5% Triton-X for fifteen minutes. Subsequently, cells were blocked in 3% BSA for one hour and then incubated with primary antibodies overnight at 4°C. After the treatment with primary antibodie,s the cells were washed 3 times with PBST and incubated for 1hour at room temperature with the appropriate secondary antibodies. Subsequently, cells were washed 3 times in PBST and incubated with 1μg/ml DAPI in PBS for 5 minutes. Images were acquired using a Leica SP5 confocal microscope with LAS X software or Olympus IX70 microscope with Micromanager software. Images were analysed with Fiji ImageJ software. CellProfiler software was used for the analysis of images from H1299 and A549 cancer cells.

Expression plasmids

Full length Cnot3 cDNA (OriGene) was cloned in pCDNA 3.2/V5/GW/D-TOPO by PCR addition of restriction sites SmaI/NotI following the manufacturer's instructions. Single Cnot3-T292A, Cnot3-S294A mutant constructs and the T292A/S294A double mutant were generated by site directed mutagenesis and cloned as above. An 8 μg aliquot of each DNA construct was transfected into HEK 293 cells by Calcium Phosphate method. Deletion fragments Cnot3 Δ1-200, Cnot3 Δ651-700, Cnot3 Δ701-751, Cnot3 Δ651-751 were synthesized (Genewiz) and cloned in pCDNA 3.2/V5/GW/D-TOPO using restriction sites KpnI/AscI.

pCDNA3-T7-ERK1 (Addgene: 14440) and full length Aurora B cDNA (Dharmacon-Horizon Discovery)was cloned in pGEX-4T1.

Immunoprecipitation (IP)

Cells were harvested in IP Lysis Buffer (50 mM Tris-HCl, pH 7.4, 150 mM NaCl, 10% glycerol, 1% Nonidet P-40, 1.0 mM EDTA) with Complete™ protease inhibitor cocktail (Merck). In all cases, 500 μg of total protein was used. The IP procedure was performed using Protein A Sepharose CL-4B beads (GE Healthcare). The extract was pre-cleared with pre-blocked beads (blocked with 1% BSA) for two hours followed by incubation with the desired primary antibodies overnight at 4°C. On the following day, beads were added to it and incubated for another four hours followed by washing the beads twice with wash buffer (50 mM Tris-cl, pH 7.4, 150 mM NaCl, 10% glycerol, 0.5% Nonidet P-40, 1.0 mM EDTA). The immunocomplexes were eluted by boiling with 2x SDS loading buffer.

Protein extractions from cells

To obtain the whole cell extracts, cells were washed with ice cold PBS and the cell pellet was reuspended in Tris lysis buffer (50 mM Tris/HCl pH 7.5, 150 mM NaCl, 1% Triton X-100, 1 mM DTT, 1 mM Na_3VO_4) with Complete™ protease inhibitor cocktail (Merck).

For preparation of cytoplasmic and nuclear extracts, cells were harvested and re-suspended in harvest buffer containing 10 mM HEPES (pH 7.9), 50 mM NaCl, 0.5 M Sucrose, 0.1 mM EDTA, 0.5% Triton-X 100 and with Complete™ protease inhibitor cocktail (Merck). After obtaining the cytoplasmic extract, the nuclear pellet was further washed with wash buffer/Buffer A (10 mM HEPES (pH 7.9), 10 mM KCL, 0.1 mM EDTA and 0.1 mM EGTA), then re-suspended in Buffer C

(10 mM HEPES (pH 7.9), 500 mM NaCl, 0.1 mM EDTA, 0.1 mM EGTA, 0.1% NP40 and protease inhibitor cocktail to extract the nuclear proteins.

Concentrations of the extracts were measured with the Bradford reagent (Bio-Rad).

Immunoblotting

Extracts were diluted in 5x SDS loading buffer, boiled for 5 min and subjected to SDS PAGE. Gels were transferred to nitrocellulose membranes using a Bio-Rad wet tank blotting system. Membranes were blocked with 5% bovine serum albumin (BSA) or 5% milk in TBS+ 0.1% Tween-20 (TBS-T) for 1hour at room temperature and incubated with the primary antibody diluted in 2.5% BSA TBS-T overnight at 4°C. On the following day, membranes were washed 3 times for 20 min with TBS-T, incubated with the appropriate secondary antibody (dilution 1:10000) for 1hour at room temperature, washed again 3 times for 15 minutes and developed using Millipore Crescendo ECL (Merck) using X ray films on Photon Imaging System or Amersham Imager 680.

Protein purification in bacteria

pGEX-4T1-Aurora B and pGEX-4T1-ERK1 were transformed into competent BL21 E.coli cells. To induce protein expression, β-D-1 thiogalactopyranoside (IPTG) (Merck) was added at a concentration of 0.5 mM and the cells were grown for 3 hours at 37°C. The cell pellets were resuspended in PBS+0.5% Triton-X 100 supplemented with Complete™ protease inhibitor cocktail (Merck) and frozen overnight at -80 °C for lysis. The following day, the mix was incubated with Lysozome (1mg/ml) followed by sonication at intervals of 15 seconds on and 45 seconds off for 5 minutes. The clear supernatants were collected and Sepharose High performance (GSH) beads (GE Healthcare), pre-washed in PBS

was added followed by overnight incubation at 4°C. Beads were washed with PBS+0.5% Triton-X 100 and the GST fusion proteins were eluted with elution buffer (10mM glutathione reduced, 5% glycerol in 50 mM Tris-Cl pH 8.0) for 15 minutes at room temperature followed by dialysis in 50 mM Tris-Cl pH 8.0, 0.15 M NaCl, 10% glycerol, 0.5 mM DTT and 0.5mM PMSF.

GST pulldown assay

In order to perform the GST pulldown with GST-Aurora B and GST-ERK1 with Cnot3 and the deletion mutants of Cnot3, pCDNA-*Cnot3*, pCDNA-Cnot3 Δ1-200, pCDNA-Cnot3 Δ651-700, pCDNA-Cnot3 Δ701-751 and pCDNA-Cnot3 Δ651-751 were *in vitro* transcribed/translated using a TNT® Quick Coupled Transcription/Translation kit (Promega) according to manufacturer's instructions. An aliquot (0.5 μg) of the plasmid was incubated with 20 μl of TNT T7 quick Master Mix, 1 μl (10μCi) of ^{35}S-Methionine and water to a final volume of 25 μl. The transcription/translation reaction was performed for 90 minutes at 30°C. 1μg of GST or GST-Aurora B or GST-ERK was added to GSH beads in binding buffer (50 mM Tris-cl pH 8.0, 150 mM monopotassium glutamate, 1mM EDTA, 0.1 % Igepal CAL630, 5% glycerol, 0.2% BSA) and supplemented with Complete™ protease inhibitor cocktail (Merck), and incubated for two hours at 4°C. The beads were then washed and 5 μl of the *in vitro* transcribed/translated CNOT3 was incubated with the beads overnight at 4°C. The beads were then washed with the binding buffer and the proteins were eluted by boiling in loading buffer. The eluted proteins were subjected to SDS-PAGE, stained, dried for one hour at 80°C and exposed overnight to Phosphor screen in a cassette (GE healthcare). Images were captured in Fujifilm FLA 5100 scanner using the Fujifilm FLA-5000 software.

***In vitro* kinase assay**

pCDNA-Cnot3-T292A, pCDNA-Cnot3-S294A, pCDNA-T292A/S294A and pCDNA-Cnot3 Δ651-751 constructs were *in vitro* transcribed/translated as described above and the resultant V5 tagged proteins were purified using V5-tagged protein purification kit ver.2 (MBL International). Purified proteins were used as substrate and incubated with 80 ng of GST-Aurora B (ProQuinase) for 30 min at 30°C in phosphorylation buffer (50 mM TrisHCl pH 7.5, 10 mM $MgCl_2$, 500 μM ATP, 1 mM DTT, 5 mM NaF, 1 μl of $^{32}P\gamma$-ATP 10μCi). Reactions were stopped by addition of SDS loading buffer, boiled for 5 min and subsequently run on SDS PAGE. The gel was dried and exposed to X ray film.

Flow cytometry

Cells were trypsinised, washed twice with PBS, fixed with 70% ethanol for 30 min on ice and washed twice with 2% FCS-PBS. Subsequently, cells were resuspended in PBS containing 1μg/ml RNAse A (Thermo Fisher Scientific), 50 μg/ml propidium iodide and 0.05% NP40, incubated 20 min at room temperature in the dark followed by analysis. Anaysis was performed on an LSRII Flow Cytometer (Becton-Dickinson) and data was analysed using FlowJo Software.

RNA sequencing

Total RNA was extracted from $2x10^6$ cells (3 biological replicates for wild-type and CNOT3-DM cells) using Trizol reagent (Thermo Fisher Scientific) following the manufacturer's instructions. A 2 μl aliquot of a 1:10 dilution of the ERCC RNA Spike-in Mix (Thermo Fisher Scientific) were added to each sample. The quality of the extracted RNA was analysed using the RNA 6000 Nano kit on a 2100 Bioanalyzer (Agilent). An aliquot of 500 ng of RNA was used to prepare a polyadenylated RNA library with the TruSeq Stranded mRNA Library Prep Kit

(Illumina) following the manufacturer's protocol. RNA libraries were sequenced in one lane by multiplexing on an Illumina HiSeq 2500 sequencer with a 100 bp read output. RNAseq reads were aligned against to Ensembl Mouse genome (NCBIM37) reference sequence assembly and transcript annotation that obtained from Illumina iGenomes (https://support.illumina.com/sequencing/sequencing_software/igenome.html) and to ERCC reference with Tophat2 (2.0.11) (Kim et al., 2013). Gene-based read counts and ERCC counts were obtained using featureCounts function from Rsubread Bioconductor package (Liao et al., 2013; Liao et al., 2014). Differentially expressed gene analysis was performed with DESeq2 Bioconductor package (Love et al., 2014) after normalising the data against ERCC with RUVseq Bioconductor package (Risso et al., 2014). Differentially expressed genes were defined with Benjamini-Hochberg adjusted p-value<0.05 and fold change ratio > 1.5. Gene ontology analysis was performed with goseq Bioconductor package (Young et al., 2010). After converting mouse gene symbol to human gene symbol using the report of Human and Mouse Homology retrieved from Mouse Genome Informatics (MGI, www.informatics.jax.org), Gene Set Enrichment Analysis (GSEA) (Mootha et al., 2003; Subramanian et al., 2005) was then performed with GseaPreranked tool using Hallmarks gene set (h.all.v5.2.symbols.gmt).

Proximity ligation assay (PLA)

PLA was performed using the Duolink In Situ Red Starter Kit Mouse/Rabbit (Merck) following manufacturer's instructions. Cells were fixed and permeabilised following standard conditions as described above followed by incubation with blocking buffer (provided in the kit) for one hour at 37°C. Subsequently, cells were incubated with desired antibodies and single antibody

controls overnight at 4°C. After the primary antibodies, the cells were washed with wash buffers and incubated with mouse and rabbit probes for one hour at 37°C followed by ligation reaction at 37°C for half an hour. The amplification reaction of the ligated product was then carried out at 37°C for 90 minutes followed by counterstaining with FITC-αTubulin for forty minutes at room temperature. The cells were finally washed and incubated with 1μg/ml DAPI in PBS for 5 minutes. Images were acquired using a Leica SP5 confocal microscope with LAS X software. PLA dots were analysed and quantified using Imaris - Bitplane software (Oxford Instruments). Three-dimensional segmentation and digital image reconstructions of the cells were carried out using Imaris Spots and Surfaces packages.

Mass spectrometry

Peptides were separated using an Ultimate 3000 RSLC nano liquid chromatography system (Thermo Fisher Scientific) coupled to an LTQ Velos Orbitrap mass spectrometer (Thermo Fisher Scientific) via a Dionex nano-esi source. Eluted peptides were analysed by the LTQ Velos operating in positive polarity using a data-dependent acquisition mode. Ions for fragmentation were determined from an initial MS1 survey scan at 60000 resolution (at m/z 200). Ion Trap CID (collisional induced dissociation), Ion Trap CID-MSA (MultiStage Activation) and HCD (Higher energy collisional induced dissociation) were carried out concurrently on the top 3 most abundant ions. For CID fragmentation methods MS1 and MS2 MSn AGC targets set to 1e6 and 1e4 for 1 microscan and a maximum injection time of 500ms and 100ms respectively. A survey scan m/z range of 350 – 1500 was used, with a normalised collision energy set to 35% for

both CID and HCD, charge state rejection enabled for +1 ions and a minimum threshold for triggering fragmentation of 500 counts.

RNA isolation and quantitative RT-PCR (qPCR)

Total RNA was isolated with TRIzol reagent (Thermo Fisher Scientific) following manufacturer's instructions. cDNA was synthesized with RevertAid First Strand cDNA Synthesis Kit (Thermo Fisher Scientific) using 200 ng of RNA following the manufacturer's protocol. qPCRs were performed using Sensimix SYBR NORox SYBR GREEN (Bioline). Each PCR was performed in duplicate using 1 μl of cDNA (from 20 μl reaction) and 200 nM primer concentration.

Gene expression was determined relative to *MLN 51* transcript levels. The primers used in this analysis are listed in Supplementary Table 1.

Statistical analysis

All statistical analyses were performed with GraphPad Prism software. The statistical tests used in each experiment and significances are indicated in the corresponding figure legends.

ACKNOWLEDGEMENTS

We thank Nicola Festuccia, Aida di Gregorio and Sheila Xie for advice and helpful discussions, Holger Kramer and Alex Montoya for assistance with mass spectrometry data analysis and Lepakshi Ranjha for advice on the ^{35}S pull-down and in vitro kinase assays. We also thank the staff of the LMS Genomics Facility for HT sequencing, and the LMS/NIHR Imperial Biomedical Research Centre Flow Cytometry Facility for support. This research was funded by the Medical Research Council UK.

The authors declare no competing interests.

Author contributions: MS, MM, MRT and ND participated in the design of the study. MS identified and characterised the effects of the Cnot3 mutations on mesendodermal differentiation and ERK phosphorylation. MM and MRT carried out the CRISPR targeting in ESCs and the initial characterisation of the nuclear localisation of CNOT3. YFW analysed the RNA-seq data. CW and DD provided microscopy expertise and carried out the digital analysis of the PLA data. PS contributed to the ESC analysis. MS and ND wrote the manuscript with contributions from MM and MRT. ND supervised and coordinated the project.

REFERENCES

Alexanian, M., D. Maric, S.P. Jenkinson, M. Mina, C.E. Friedman, C.-C. Ting, R. Micheletti, I. Plaisance, M. Nemir, D. Maison, J. Kernen, I. Pezzuto, D. Villeneuve, F. Burdet, M. Ibberson, S.L. Leib, N.J. Palpant, N. Hernandez, S. Ounzain, and T. Pedrazzini. 2017. A transcribed enhancer dictates mesendoderm specification in pluripotency. *Nature Communications*. 8:1806.

Bakre, M.M., A. Hoi, J.C. Mong, Y.Y. Koh, K.Y. Wong, and L.W. Stanton. 2007. Generation of multipotential mesendodermal progenitors from mouse embryonic stem cells via sustained Wnt pathway activation. *J Biol Chem*. 282:31703-31712.

Bang, Y.J., J.H. Kwon, S.H. Kang, J.W. Kim, and Y.C. Yang. 1998. Increased MAPK activity and MKP-1 overexpression in human gastric adenocarcinoma. *Biochem Biophys Res Commun*. 250:43-47.

Ben-Haim, N., C. Lu, M. Guzman-Ayala, L. Pescatore, D. Mesnard, M. Bischofberger, F. Naef, E.J. Robertson, and D.B. Constam. 2006. The nodal precursor acting via activin receptors induces mesoderm by maintaining a source of its convertases and BMP4. *Developmental cell*. 11:313-323.

Bernardo, A.S., T. Faial, L. Gardner, K.K. Niakan, D. Ortmann, C.E. Senner, E.M. Callery, M.W. Trotter, M. Hemberger, J.C. Smith, L. Bardwell, A. Moffett, and R.A. Pedersen. 2011. BRACHYURY and CDX2 mediate BMP-induced differentiation of human and mouse pluripotent stem cells into embryonic and extraembryonic lineages. *Cell stem cell*. 9:144-155.

Bertocchini, F., and C.D. Stern. 2002. The hypoblast of the chick embryo positions the primitive streak by antagonizing nodal signaling. *Developmental cell*. 3:735-744.

Boland, A., Y. Chen, T. Raisch, S. Jonas, D. Kuzuoglu-Ozturk, L. Wohlbold, O. Weichenrieder, and E. Izaurralde. 2013. Structure and assembly of the NOT module of the human CCR4-NOT complex. *Nature structural & molecular biology*. 20:1289-1297.

Bonet, C., S. Giuliano, M. Ohanna, K. Bille, M. Allegra, J.P. Lacour, P. Bahadoran, S. Rocchi, R. Ballotti, and C. Bertolotto. 2012. Aurora B is regulated by the mitogen-activated protein kinase/extracellular signal-regulated kinase (MAPK/ERK) signaling pathway and is a valuable potential target in melanoma cells. *J Biol Chem*. 287:29887-29898.

Carmena, M., M. Wheelock, H. Funabiki, and W.C. Earnshaw. 2012. The chromosomal passenger complex (CPC): from easy rider to the godfather of mitosis. *Nat Rev Mol Cell Biol*. 13:789-803.

Caunt, Christopher J., and Craig A. McArdle. 2012. ERK phosphorylation and nuclear accumulation: insights from single-cell imaging. *Biochemical Society transactions*. 40:224-229.

Cejas, P., A. Cavazza, C.N. Yandava, V. Moreno, D. Horst, J. Moreno-Rubio, E. Burgos, M. Mendiola, L. Taing, A. Goel, J. Feliu, and R.A. Shivdasani. 2017. Transcriptional Regulator CNOT3 Defines an Aggressive Colorectal Cancer Subtype. *Cancer Res*. 77:766-779.

Chuai, M., D. Hughes, and C.J. Weijer. 2012. Collective epithelial and mesenchymal cell migration during gastrulation. *Curr Genomics*. 13:267-277.

Ciruna, B., and J. Rossant. 2001. FGF signaling regulates mesoderm cell fate specification and morphogenetic movement at the primitive streak. *Developmental cell*. 1:37-49.

Collart, M.A. 2016. The Ccr4-Not complex is a key regulator of eukaryotic gene expression. *Wiley Interdiscip Rev RNA*. 7:438-454.

Costello, I., S. Nowotschin, X. Sun, A.W. Mould, A.K. Hadjantonakis, E.K. Bikoff, and E.J. Robertson. 2015. Lhx1 functions together with Otx2, Foxa2, and Ldb1 to govern anterior mesendoderm, node, and midline development. *Genes Dev*. 29:2108-2122.

De Keersmaecker, K., Z.K. Atak, N. Li, C. Vicente, S. Patchett, T. Girardi, V. Gianfelici, E. Geerdens, E. Clappier, M. Porcu, I. Lahortiga, R. Luca, J. Yan, G. Hulselmans, H. Vranckx, R. Vandepoel, B. Sweron, K. Jacobs, N. Mentens, I. Wlodarska, B. Cauwelier, J. Cloos, J. Soulier, A. Uyttebroeck, C. Bagni, B.A. Hassan, P. Vandenberghe, A.W. Johnson, S. Aerts, and J. Cools. 2013. Exome sequencing identifies mutation in CNOT3 and ribosomal genes RPL5 and RPL10 in T-cell acute lymphoblastic leukemia. *Nat Genet*. 45:186-190.

Delacruz, R.G.C., I.T. Sandoval, K. Chang, B.N. Miller, L. Reyes-Uribe, E. Borras, P.M. Lynch, M.W. Taggart, E.T. Hawk, E. Vilar, and D.A. Jones. 2019. Functional characterization of CNOT3 variants identified in familial adenomatous polyposis adenomas. *Oncotarget*. 10:3939-3951.

Deng, C.X., A. Wynshaw-Boris, M.M. Shen, C. Daugherty, D.M. Ornitz, and P. Leder. 1994. Murine FGFR-1 is required for early postimplantation growth and axial organization. *Genes Dev*. 8:3045-3057.

Deschenes-Simard, X., M.F. Gaumont-Leclerc, V. Bourdeau, F. Lessard, O. Moiseeva, V. Forest, S. Igelmann, F.A. Mallette, M.K. Saba-El-Leil, S. Meloche, F. Saad, A.M. Mes-Masson, and G. Ferbeyre. 2013. Tumor suppressor activity of the ERK/MAPK pathway by promoting selective protein degradation. *Genes Dev*. 27:900-915.

Dixon, S.E., M.M. Bhatti, V.N. Uversky, A.K. Dunker, and W.J. Sullivan, Jr. 2011. Regions of intrinsic disorder help identify a novel nuclear localization

signal in Toxoplasma gondii histone acetyltransferase TgGCN5-B. *Mol Biochem Parasitol*. 175:192-195.
Donchet, A., J. Oliva, A. Labaronne, L. Tengo, M. Miloudi, C.A.G. F, C. Mas, G. Schoehn, W.H.R. R, M. Ducatez, and T. Crepin. 2019. The structure of the nucleoprotein of Influenza D shows that all Orthomyxoviridae nucleoproteins have a similar NPCORE, with or without a NPTAIL for nuclear transport. *Scientific reports*. 9:600.
Forbes, S.A., D. Beare, H. Boutselakis, S. Bamford, N. Bindal, J. Tate, C.G. Cole, S. Ward, E. Dawson, L. Ponting, R. Stefancsik, B. Harsha, C.Y. Kok, M. Jia, H. Jubb, Z. Sondka, S. Thompson, T. De, and P.J. Campbell. 2017. COSMIC: somatic cancer genetics at high-resolution. *Nucleic Acids Res*. 45:D777-D783.
Frangini, A. 2013. Characterization of the role of Aurora B kinase in quiescent lymphocytes. Vol. PhD. Imperial College London.
Fujiwara, T., D.B. Dehart, K.K. Sulik, and B.L. Hogan. 2002. Distinct requirements for extra-embryonic and embryonic bone morphogenetic protein 4 in the formation of the node and primitive streak and coordination of left-right asymmetry in the mouse. *Development*. 129:4685-4696.
Georgopoulos, N.T., L.A. Kirkwood, and J. Southgate. 2014. A novel bidirectional positive-feedback loop between Wnt-beta-catenin and EGFR-ERK plays a role in context-specific modulation of epithelial tissue regeneration. *J Cell Sci*. 127:2967-2982.
Giannakis, M., X.J. Mu, S.A. Shukla, Z.R. Qian, O. Cohen, R. Nishihara, S. Bahl, Y. Cao, A. Amin-Mansour, M. Yamauchi, Y. Sukawa, C. Stewart, M. Rosenberg, K. Mima, K. Inamura, K. Nosho, J.A. Nowak, M.S. Lawrence, E.L. Giovannucci, A.T. Chan, K. Ng, J.A. Meyerhardt, E.M. Van Allen, G. Getz, S.B. Gabriel, E.S. Lander, C.J. Wu, C.S. Fuchs, S. Ogino, and L.A. Garraway. 2016. Genomic Correlates of Immune-Cell Infiltrates in Colorectal Carcinoma. *Cell reports*. 15:857-865.
Hornbeck, P.V., B. Zhang, B. Murray, J.M. Kornhauser, V. Latham, and E. Skrzypek. 2015. PhosphoSitePlus, 2014: mutations, PTMs and recalibrations. *Nucleic Acids Res*. 43:D512-520.
Hu, G., J. Kim, Q. Xu, Y. Leng, S.H. Orkin, and S.J. Elledge. 2009. A genome-wide RNAi screen identifies a new transcriptional module required for self-renewal. *Genes Dev*. 23:837-848.
Jeong, W.-J., E.J. Ro, and K.-Y. Choi. 2018. Interaction between Wnt/β-catenin and RAS-ERK pathways and an anti-cancer strategy via degradations of β-catenin and RAS by targeting the Wnt/β-catenin pathway. *npj Precision Oncology*. 2:5.
Kim, D., G. Pertea, C. Trapnell, H. Pimentel, R. Kelley, and S.L. Salzberg. 2013. TopHat2: accurate alignment of transcriptomes in the presence of insertions, deletions and gene fusions. *Genome biology*. 14:R36.
Kim, J.S., B.S. Kim, J. Kim, C.S. Park, and I.Y. Chung. 2010. The phosphoinositide-3-kinase/Akt pathway mediates the transient increase in Nanog expression during differentiation of F9 cells. *Arch Pharm Res*. 33:1117-1125.
Kolch, W. 2005. Coordinating ERK/MAPK signalling through scaffolds and inhibitors. *Nat Rev Mol Cell Biol*. 6:827-837.
Kunath, T., M.K. Saba-El-Leil, M. Almousailleakh, J. Wray, S. Meloche, and A. Smith. 2007. FGF stimulation of the Erk1/2 signalling cascade triggers

transition of pluripotent embryonic stem cells from self-renewal to lineage commitment. *Development*. 134:2895-2902.
Lanner, F., and J. Rossant. 2010. The role of FGF/Erk signaling in pluripotent cells. *Development*. 137:3351-3360.
Li, X., M. Morita, C. Kikuguchi, A. Takahashi, T. Suzuki, and T. Yamamoto. 2017. Adipocyte-specific disruption of mouse Cnot3 causes lipodystrophy. *FEBS Lett*. 591:358-368.
Liao, Y., G.K. Smyth, and W. Shi. 2013. The Subread aligner: fast, accurate and scalable read mapping by seed-and-vote. *Nucleic Acids Res*. 41:e108.
Liao, Y., G.K. Smyth, and W. Shi. 2014. featureCounts: an efficient general purpose program for assigning sequence reads to genomic features. *Bioinformatics (Oxford, England)*. 30:923-930.
Love, M.I., W. Huber, and S. Anders. 2014. Moderated estimation of fold change and dispersion for RNA-seq data with DESeq2. *Genome biology*. 15:550.
Mebratu, Y., and Y. Tesfaigzi. 2009. How ERK1/2 activation controls cell proliferation and cell death: Is subcellular localization the answer? *Cell Cycle*. 8:1168-1175.
Mootha, V.K., C.M. Lindgren, K.F. Eriksson, A. Subramanian, S. Sihag, J. Lehar, P. Puigserver, E. Carlsson, M. Ridderstrale, E. Laurila, N. Houstis, M.J. Daly, N. Patterson, J.P. Mesirov, T.R. Golub, P. Tamayo, B. Spiegelman, E.S. Lander, J.N. Hirschhorn, D. Altshuler, and L.C. Groop. 2003. PGC-1alpha-responsive genes involved in oxidative phosphorylation are coordinately downregulated in human diabetes. *Nat Genet*. 34:267-273.
Neely, G.G., K. Kuba, A. Cammarato, K. Isobe, S. Amann, L. Zhang, M. Murata, L. Elmen, V. Gupta, S. Arora, R. Sarangi, D. Dan, S. Fujisawa, T. Usami, C.P. Xia, A.C. Keene, N.N. Alayari, H. Yamakawa, U. Elling, C. Berger, M. Novatchkova, R. Koglgruber, K. Fukuda, H. Nishina, M. Isobe, J.A. Pospisilik, Y. Imai, A. Pfeufer, A.A. Hicks, P.P. Pramstaller, S. Subramaniam, A. Kimura, K. Ocorr, R. Bodmer, and J.M. Penninger. 2010. A global in vivo Drosophila RNAi screen identifies NOT3 as a conserved regulator of heart function. *Cell*. 141:142-153.
Nichols, J., J. Silva, M. Roode, and A. Smith. 2009. Suppression of Erk signalling promotes ground state pluripotency in the mouse embryo. *Development*. 136:3215-3222.
Pouysségur, J., and P. Lenormand. 2003. Fidelity and spatio-temporal control in MAP kinase (ERKs) signalling. *European Journal of Biochemistry*. 270:3291-3299.
Priestley, P., J. Baber, M.P. Lolkema, N. Steeghs, E. de Bruijn, C. Shale, K. Duyvesteyn, S. Haidari, A. van Hoeck, W. Onstenk, P. Roepman, M. Voda, H.J. Bloemendal, V.C.G. Tjan-Heijnen, C.M.L. van Herpen, M. Labots, P.O. Witteveen, E.F. Smit, S. Sleijfer, E.E. Voest, and E. Cuppen. 2019. Pan-cancer whole-genome analyses of metastatic solid tumours. *Nature*.
Risso, D., J. Ngai, T.P. Speed, and S. Dudoit. 2014. Normalization of RNA-seq data using factor analysis of control genes or samples. *Nature biotechnology*. 32:896-902.
Roskoski, R., Jr. 2012. ERK1/2 MAP kinases: structure, function, and regulation. *Pharmacol Res*. 66:105-143.

Roux, P.P., and J. Blenis. 2004. ERK and p38 MAPK-activated protein kinases: a family of protein kinases with diverse biological functions. *Microbiol Mol Biol Rev*. 68:320-344.
Sacks, D.B. 2006. The role of scaffold proteins in MEK/ERK signalling. *Biochemical Society transactions*. 34:833-836.
Sasai, K., H. Katayama, D.H. Hawke, and S. Sen. 2016. Aurora-C Interactions with Survivin and INCENP Reveal Shared and Distinct Features Compared with Aurora-B Chromosome Passenger Protein Complex. *PLoS One*. 11:e0157305.
Sebolt-Leopold, J.S., D.T. Dudley, R. Herrera, K. Van Becelaere, A. Wiland, R.C. Gowan, H. Tecle, S.D. Barrett, A. Bridges, S. Przybranowski, W.R. Leopold, and A.R. Saltiel. 1999. Blockade of the MAP kinase pathway suppresses growth of colon tumors in vivo. *Nat Med*. 5:810-816.
Shirai, Y.T., A. Mizutani, S. Nishijima, M. Horie, C. Kikuguchi, O. Elisseeva, and T. Yamamoto. 2019. CNOT3 targets negative cell cycle regulators in non-small cell lung cancer development. *Oncogene*. 38:2580-2594.
Smith, B.N., L.J. Burton, V. Henderson, D.D. Randle, D.J. Morton, B.A. Smith, L. Taliaferro-Smith, P. Nagappan, C. Yates, M. Zayzafoon, L.W. Chung, and V.A. Odero-Marah. 2014. Snail promotes epithelial mesenchymal transition in breast cancer cells in part via activation of nuclear ERK2. *PLoS One*. 9:e104987.
Song, J., S. Salek-Ardakani, T. So, and M. Croft. 2007. The kinases aurora B and mTOR regulate the G1-S cell cycle progression of T lymphocytes. *Nat Immunol*. 8:64-73.
Stern, C.D., and K.M. Downs. 2012. The hypoblast (visceral endoderm): an evo-devo perspective. *Development*. 139:1059-1069.
Subramanian, A., P. Tamayo, V.K. Mootha, S. Mukherjee, B.L. Ebert, M.A. Gillette, A. Paulovich, S.L. Pomeroy, T.R. Golub, E.S. Lander, and J.P. Mesirov. 2005. Gene set enrichment analysis: a knowledge-based approach for interpreting genome-wide expression profiles. *Proc Natl Acad Sci U S A*. 102:15545-15550.
Takeshita, M., T. Koga, K. Takayama, K. Ijichi, T. Yano, Y. Maehara, Y. Nakanishi, and K. Sueishi. 2013. Aurora-B overexpression is correlated with aneuploidy and poor prognosis in non-small cell lung cancer. *Lung Cancer*. 80:85-90.
Tang, Y.S., C.Y. Lo, C.K. Mok, P.K. Chan, and P.C. Shaw. 2019. The Extended C-Terminal Region of Influenza C Virus Nucleoprotein Is Important for Nuclear Import and Ribonucleoprotein Activity. *J Virol*. 93.
Trakala, M., G. Fernandez-Miranda, I. Perez de Castro, C. Heeschen, and M. Malumbres. 2013. Aurora B prevents delayed DNA replication and premature mitotic exit by repressing p21(Cip1). *Cell Cycle*. 12:1030-1041.
Tremblay, K.D., P.A. Hoodless, E.K. Bikoff, and E.J. Robertson. 2000. Formation of the definitive endoderm in mouse is a Smad2-dependent process. *Development*. 127:3079-3090.
Tsakiridis, A., Y. Huang, G. Blin, S. Skylaki, F. Wymeersch, R. Osorno, C. Economou, E. Karagianni, S. Zhao, S. Lowell, and V. Wilson. 2014. Distinct Wnt-driven primitive streak-like populations reflect in vivo lineage precursors. *Development*. 141:1209-1221.

Tuncel, H., F. Shimamoto, H. Kaneko Guangying Qi, E. Aoki, H. Jikihara, S. Nakai, T. Takata, and M. Tatsuka. 2012. Nuclear Aurora B and cytoplasmic Survivin expression is involved in lymph node metastasis of colorectal cancer. *Oncology letters*. 3:1109-1114.

Vallier, L., T. Touboul, Z. Chng, M. Brimpari, N. Hannan, E. Millan, L.E. Smithers, M. Trotter, P. Rugg-Gunn, A. Weber, and R.A. Pedersen. 2009. Early cell fate decisions of human embryonic stem cells and mouse epiblast stem cells are controlled by the same signalling pathways. *PLoS One*. 4:e6082.

Wang, L., and Y.G. Chen. 2016. Signaling Control of Differentiation of Embryonic Stem Cells toward Mesendoderm. *Journal of molecular biology*. 428:1409-1422.

Wang, Q., Y. Zhou, X. Wang, and B.M. Evers. 2006. Glycogen synthase kinase-3 is a negative regulator of extracellular signal-regulated kinase. *Oncogene*. 25:43-50.

Wolfe, A.D., and K.M. Downs. 2014. Mixl1 localizes to putative axial stem cell reservoirs and their posterior descendants in the mouse embryo. *Gene Expr Patterns*. 15:8-20.

Xu, X., M. Weinstein, C. Li, M. Naski, R.I. Cohen, D.M. Ornitz, P. Leder, and C. Deng. 1998. Fibroblast growth factor receptor 2 (FGFR2)-mediated reciprocal regulation loop between FGF8 and FGF10 is essential for limb induction. *Development*. 125:753-765.

Yamaguchi, T.P., K. Harpal, M. Henkemeyer, and J. Rossant. 1994. fgfr-1 is required for embryonic growth and mesodermal patterning during mouse gastrulation. *Genes Dev*. 8:3032-3044.

Yang, C.Y., S. Ramamoorthy, S. Boller, M. Rosenbaum, A. Rodriguez Gil, G. Mittler, Y. Imai, K. Kuba, and R. Grosschedl. 2016. Interaction of CCR4-NOT with EBF1 regulates gene-specific transcription and mRNA stability in B lymphopoiesis. *Genes Dev*. 30:2310-2324.

Young, M.D., M.J. Wakefield, G.K. Smyth, and A. Oshlack. 2010. Gene ontology analysis for RNA-seq: accounting for selection bias. *Genome biology*. 11:R14.

Yu, P., G. Pan, J. Yu, and J.A. Thomson. 2011. FGF2 sustains NANOG and switches the outcome of BMP4-induced human embryonic stem cell differentiation. *Cell stem cell*. 8:326-334.

Zhang, Y., C. Jiang, H. Li, F. Lv, X. Li, X. Qian, L. Fu, B. Xu, and X. Guo. 2015. Elevated Aurora B expression contributes to chemoresistance and poor prognosis in breast cancer. *Int J Clin Exp Pathol*. 8:751-757.

Zheng, X., R. Dumitru, B.L. Lackford, J.M. Freudenberg, A.P. Singh, T.K. Archer, R. Jothi, and G. Hu. 2012. Cnot1, Cnot2, and Cnot3 maintain mouse and human ESC identity and inhibit extraembryonic differentiation. *Stem cells (Dayton, Ohio)*. 30:910-922.

FIGURE 1

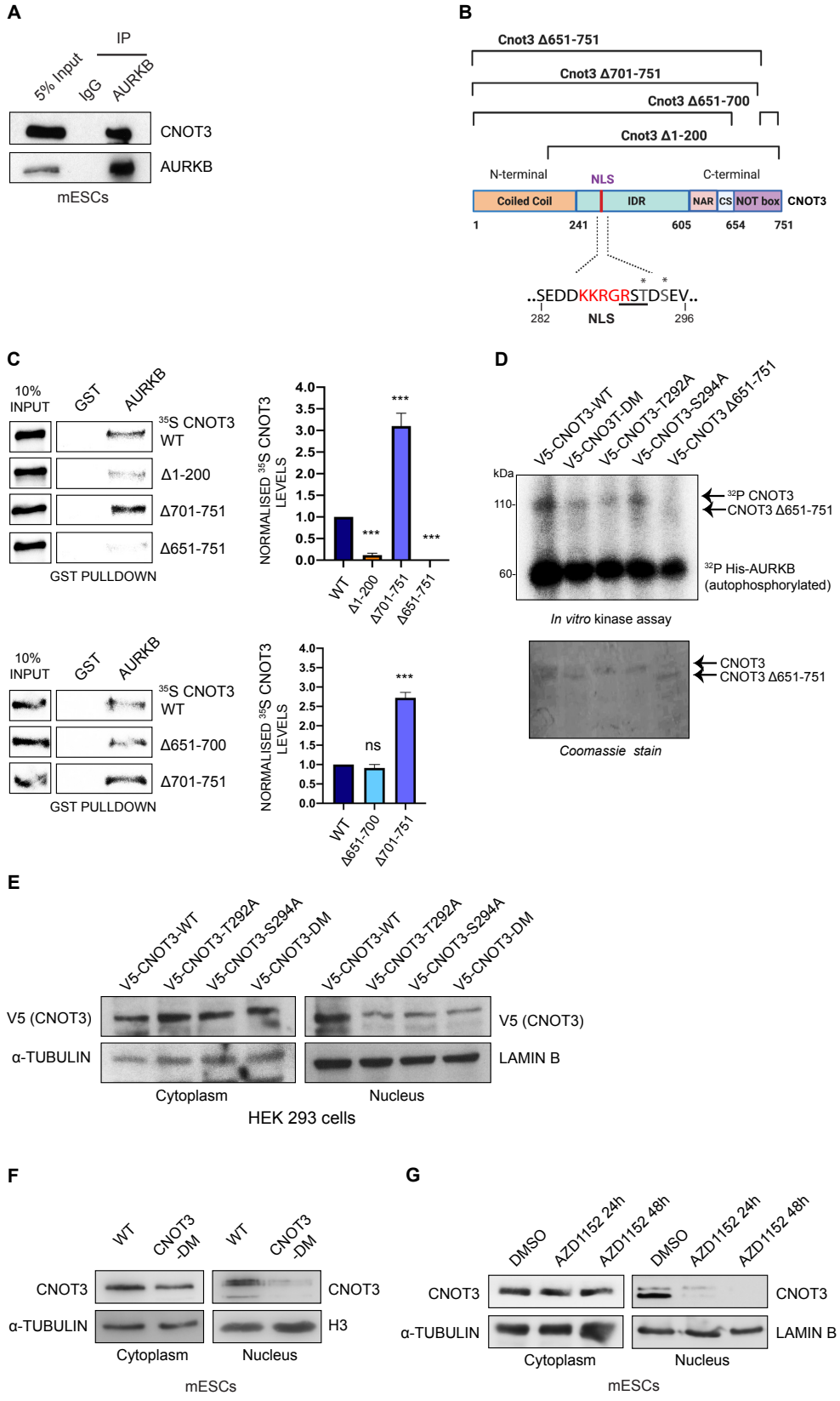
A
IP
5% Input
IgG
AURKB
CNOT3
AURKB
mESCs
B
Cnot3 Δ651-751
Cnot3 Δ701-751
Cnot3 Δ651-700
Cnot3 Δ1-200
N-terminal
NLS
C-terminal
Coiled Coil
IDR
NAR
CS
NOT box
CNOT3
1
241
605
654
751
..SEDDKKRGRSTDSEV..
282
NLS
296
C
10% INPUT
GST
AURKB
35S CNOT3 WT
Δ1-200
Δ701-751
Δ651-751
GST PULLDOWN
NORMALISED 35S CNOT3 LEVELS
WT
Δ1-200
Δ701-751
Δ651-751
10% INPUT
GST
AURKB
35S CNOT3 WT
Δ651-700
Δ701-751
GST PULLDOWN
NORMALISED 35S CNOT3 LEVELS
ns
WT
Δ651-700
Δ701-751
D
V5-CNOT3-WT
V5-CNO3T-DM
V5-CNOT3-T292A
V5-CNOT3-S294A
V5-CNOT3 Δ651-751
kDa
110
60
32P CNOT3
CNOT3 Δ651-751
32P His-AURKB (autophosphorylated)
In vitro kinase assay
CNOT3
CNOT3 Δ651-751
Coomassie stain
E
V5-CNOT3-WT
V5-CNOT3-T292A
V5-CNOT3-S294A
V5-CNOT3-DM
V5 (CNOT3)
α-TUBULIN
LAMIN B
Cytoplasm
Nucleus
HEK 293 cells
F
WT
CNOT3 -DM
CNOT3
α-TUBULIN
H3
Cytoplasm
Nucleus
mESCs
G
DMSO
AZD1152 24h
AZD1152 48h
CNOT3
α-TUBULIN
LAMIN B
Cytoplasm
Nucleus
mESCs

Figure 1: Phosphorylation by Aurora B is increases nuclear localisation of CNOT3. A. Representative immunoprecipitation (IP) carried out on cell extracts prepared from wild-type ESCs using anti-Aurora B antibody. Blots were probed with anti-CNOT3 antibody and anti-Aurora B antibody. IP with normal mouse IgG was used as a negative control. Input = 5% of the extract. **B.** Schematic representation of the organisation of the domains of CNOT3 (Boland et al., 2013) and the deletion mutants of *Cnot3* used in the GST pulldown assay. IDR = intrinsically disordered region; NAR = NOT1 anchor region; CS = connector sequence; NLS (red type) = nuclear localisation sequence. The Aurora B consensus phosphorylation site is underlined. **C.** *In vitro* GST pulldown assay using GST-Aurora B and ^{35}S-labelled *in vitro* transcribed/translated wild-type (WT) CNOT3 and CNOT3 deletion mutants (as shown in B). Top and bottom left panels: Representative pulldown assays of GST-Aurora B and ^{35}S labelled WT CNOT3 and CNOT3 deletion mutants. GST-only was used as a negative control for each pulldown. Input =10% of the respective labelled proteins. Right panels: Histograms show quantification of the band intensities normalized to input and relative to WT-CNOT3. Mean ± SEM; n=3 (unpaired t-test ***P<0.001). **D.** *In vitro* kinase assay (top) carried out on purified V5-tagged CNOT3, with single mutant constructs (CNOT3-T292A or CNOT3-S294A), the double mutant CNOT3-DM and CNOT3 Δ651-751 using γ-^{32}P-ATP. The lower band is autophosphorylated Aurora B. Coomassie stain (below) showing the levels of the respective proteins. **E.** Representative immunoblot analysis of V5-tagged CNOT3 carried out on cytoplasmic (CYT) and nuclear (NUC) extracts from HEK 293 cells transfected with WT *Cnot3*, *Cnot3*-T292A, *Cnot3*-S294A, or *Cnot3*-DM expression constructs.

Cells were harvested 48 hours post-transfection. α-Tubulin and Lamin B were used as loading controls for the cytoplasm and nucleus respectively.

F. Representative immunoblot analysis of CNOT3 levels in cytoplasmic and nuclear extracts of wild-type (WT) and *Cnot3*-DM ESCs. Cytoplasmic loading control: α-Tubulin. Nuclear loading control: Histone H3. **G.** Representative immunoblot analysis of CNOT3 from cytoplasmic and nuclear extracts of WT ESCs, treated with Aurora B inhibitor AZD1152 for 24 hours and 48 hours respectively before harvesting. DMSO: vehicle control. Cytoplasmic loading control: α-Tubulin. Nuclear loading control: Lamin B.

FIGURE 2

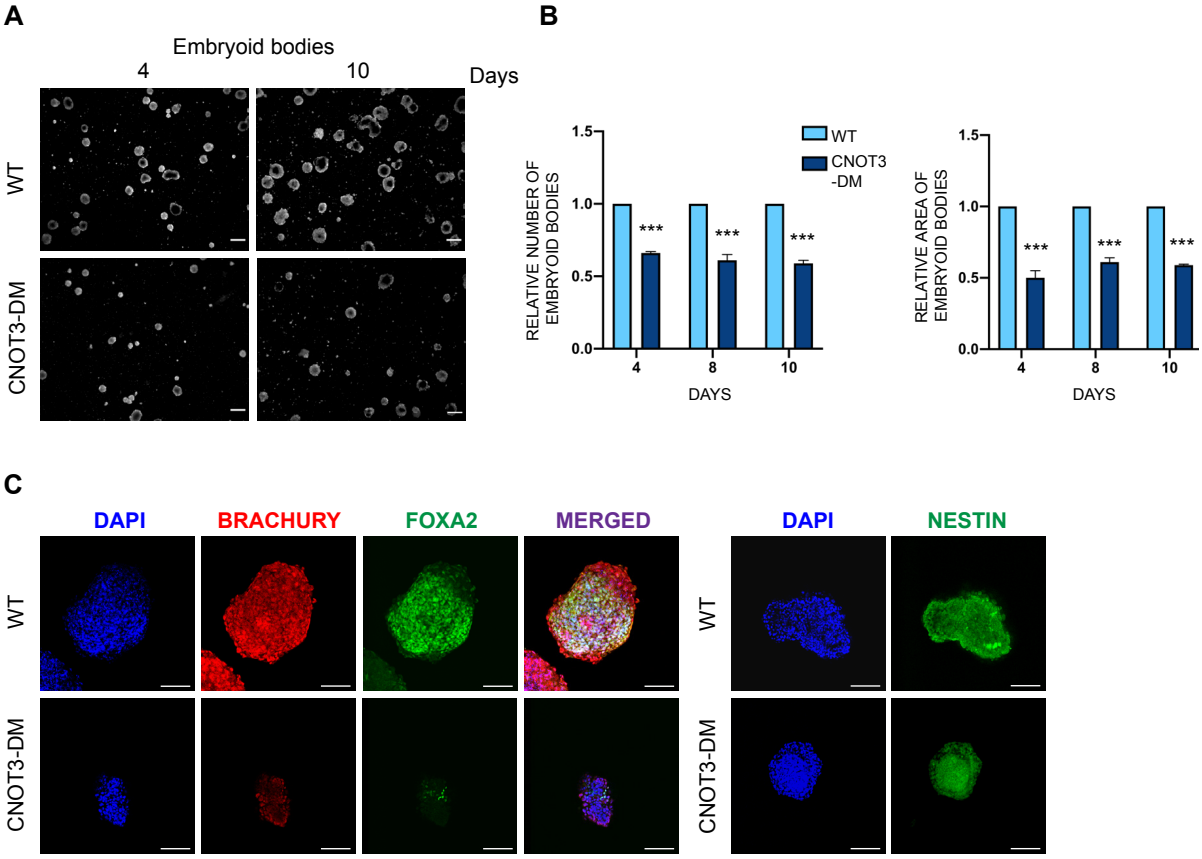

Figure 2: Mutation of CNOT3-T292A/S294 affects EB germ layer formation.

A. Representative phase-contrast images of embryoid bodies (EBs) formed from wild-type (WT) and *Cnot3*-DM ESCs after 4 and 10 days. Scale bar = 100 μm.

B. Histograms show the number (left panel) and size (right panel) of EBs formed from *Cnot3*-DM ESCs relative to WT cells at 4, 8 and 10 days respectively. Mean ± SEM; *t*-test ***P<0.001 *n*=3. **C.** Left panel: Representative confocal images of EBs derived from WT and *Cnot3*-DM ESCs stained with the mesodermal marker Brachury (red) and endodermal marker FOXA2 (green) at 8 days (scale bar = 100 μm). Right panel: staining of WT and *Cnot3*-DM EBs for ectodermal marker nestin (green) (scale bar = 100 μm). Nuclei were stained with DAPI. Staining for an additional ectodermal marker OTX2 is shown in Supplementary Figure 3A.

FIGURE 3

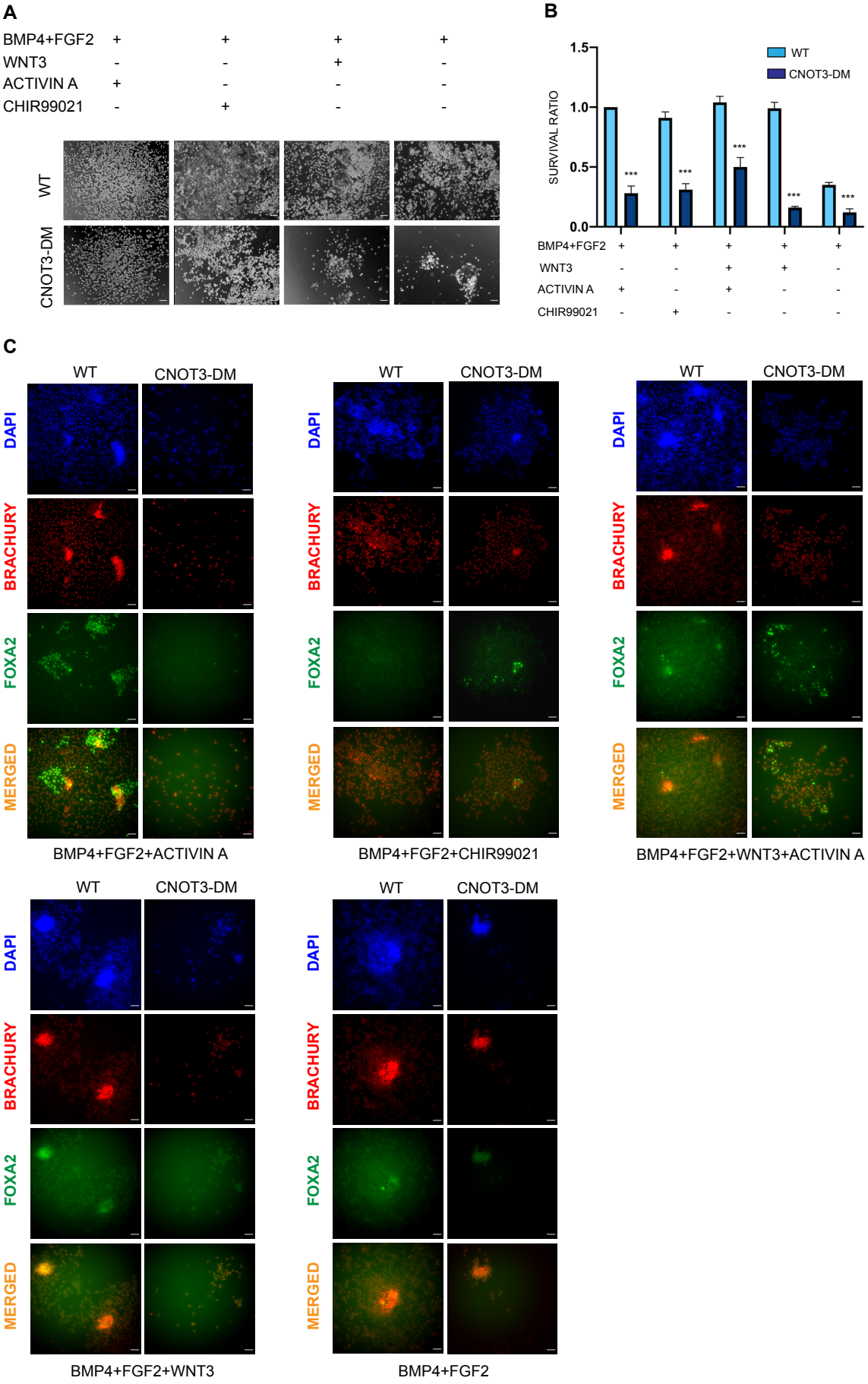
A
BMP4+FGF2 + + + +
WNT3 - - + -
ACTIVIN A + - - -
CHIR99021 - + - -
WT
CNOT3-DM
B
SURVIVAL RATIO
1.5
1.0
0.5
0.0
WT
CNOT3-DM
***
BMP4+FGF2 + + + + +
WNT3 - - + + -
ACTIVIN A + - + - -
CHIR99021 - + - - -
C
WT
CNOT3-DM
DAPI
BRACHURY
FOXA2
MERGED
BMP4+FGF2+ACTIVIN A
BMP4+FGF2+CHIR99021
BMP4+FGF2+WNT3+ACTIVIN A
BMP4+FGF2+WNT3
BMP4+FGF2
4 days mesendoderm differentiation

Figure 3: CNOT3 phosphorylation promotes efficient differentiation of ME.

A. Representative phase-contrast images showing the efficiency of mesendoderm (ME) differentiation of wild-type (WT) and *Cnot3*-DM ESCs over 4 days in the presence of various combinations (as indicated above the images) of Activin A, CHIR99021, Wnt3 and BMP4 + FGF2. Scale bar = 100 μm. **B**. Histogram shows survival of WT and *Cnot3*-DM ESCs treated with different combinations of the ligands used in (A) over 4 days of mesendoderm differentiation. Activin A, CHIR99021 or Wnt3 was added after two days of BMP4+FGF2-induced differentiation and the cell survival was determined using the WST-1 reagent on day 4 of the differentiation. Survival ratios (mean ± SEM) were calculated relative to the values obtained for WT cells treated with Activin A+ BMP4+FGF2, which was assigned a value of 1. Significance was calculated between WT and CNOT3-DM for each combination using unpaired *t*-test ***P<0.001, *n*=3. Analysis of cell survival in the presence of Activin only or Wnt only is shown Figure S3B.

C. Representative IF images of mesodermal marker Brachury (red) and endodermal marker FOXA2 (green) following mesendoderm differentiation of WT and *Cnot3*-DM ESCs for 4 days induced by combinations of BMP4 + FGF2, Activin A, CHIR99021 and Wnt3 (as indicated). Merged red and green images show the mesendodermal cells. Nuclei were stained with DAPI; scale bar = 100 μm.

FIGURE 4

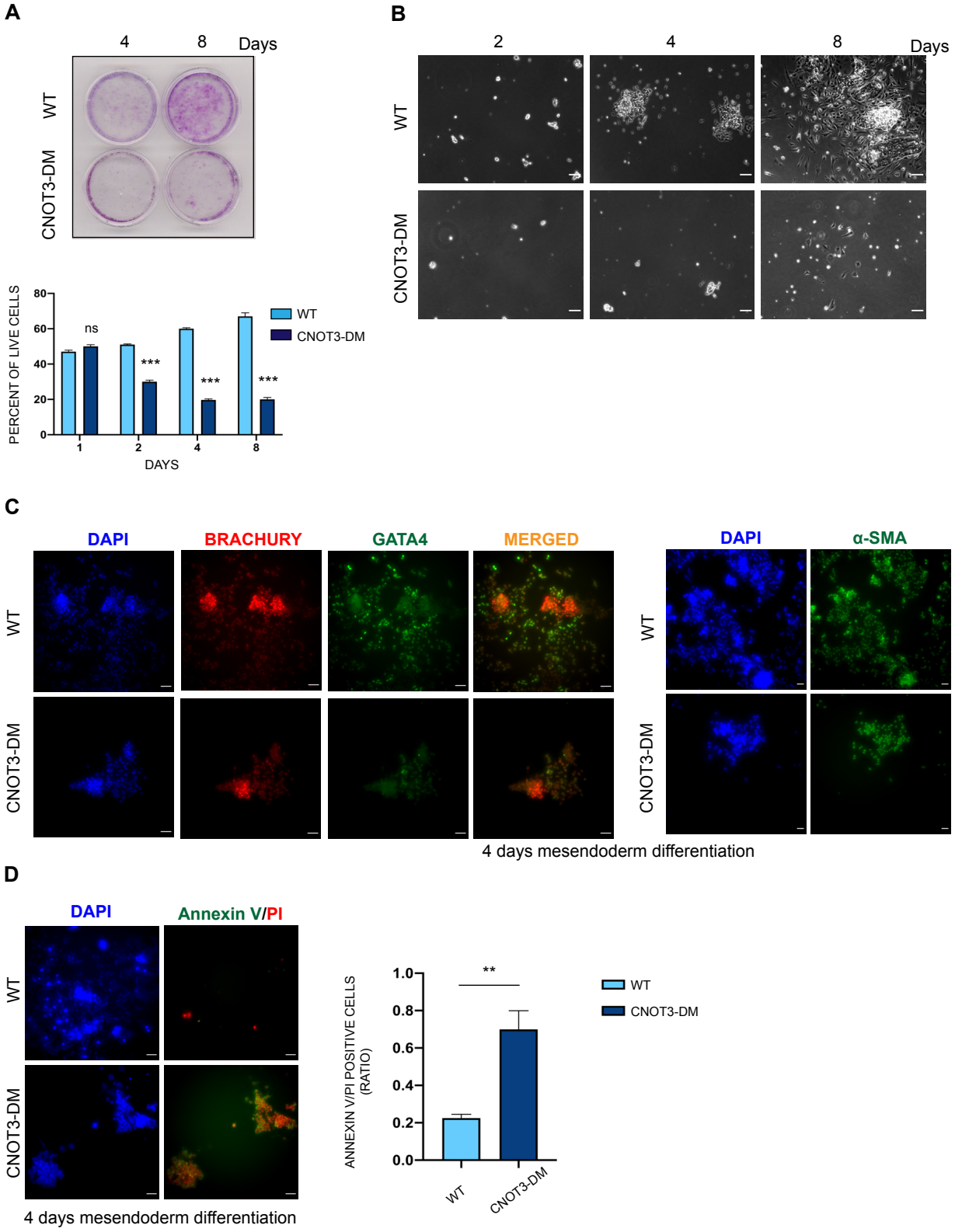

Figure 4: Phosphorylation of CNOT3 prevents apoptosis of differentiating ME cells. A. Top panel: Crystal violet staining of cells after 4 days BMP4 + FGF2-

induced mesendoderm differentiation of wild-type (WT) and *Cnot3*-DM ESCs after 4 and 8 days. Bottom panel: At the indicated time-points, live cells were counted based on trypan blue exclusion. Histogram shows the percentage of live cells at different time points of differentiation. Mean ± SEM; unpaired *t*-test between WT and *Cnot3*-DM for each time-point, ***P<0.001 *n*=3. Differentions of two other independently generated clones of *Cnot3*-T292A/S294A mutant ESCs are shown in Figure S3A. **B**. Representative phase-contrast images showing the efficiency of BMP4 + FGF2 induced mesendoderm differentiation of WT and *Cnot3*-DM ESCs for 2, 4, and 8 days. Scale bar: 100 μm. See also Supplementary Video 1 for a time-lapse analysis of the differentiations. **C**. Staining for ME markers shows that differentiation of *Cnot3*-DM ESCs with BMP4 + FGF2 for 4 days generates reduced numbers of ME cells. Left panel: Representative IF analyses of staining of differentiated cells for the mesodermal marker Brachury (red) and endodermal marker and GATA4 (green) carried out on ME cells differentiated from WT and *Cnot3*-DM ESCs by incubating them with. Right panel: staining for the additional mesodermal marker smooth muscle actin (SMA) (green). Nuclei were stained with DAPI. Merged red and green images show the ME cells. Scale bars in (C) = 100 μm; scale bar in (D) = 60 μm. For IF analysis at 8 days of differentiation, see Figure S4C and S4D. **D**. IF analysis of apoptotic markers Annexin V (green) and PI (red), in cells differentiated for 4 days with BMP4 + FGF2. Merged images show the Annexin V and PI stained apoptotic cells. Nuclei were stained with DAPI; scale bar = 100 μm. Histogram represents ratio of Annexin V/PI positive cells relative to total number of cells. Apoptotic cells were counted from ten randomly chosen fields for each biological replicate. Mean ± SEM; *t*-test **P<0.01 *n*=3.

FIGURE 5

A

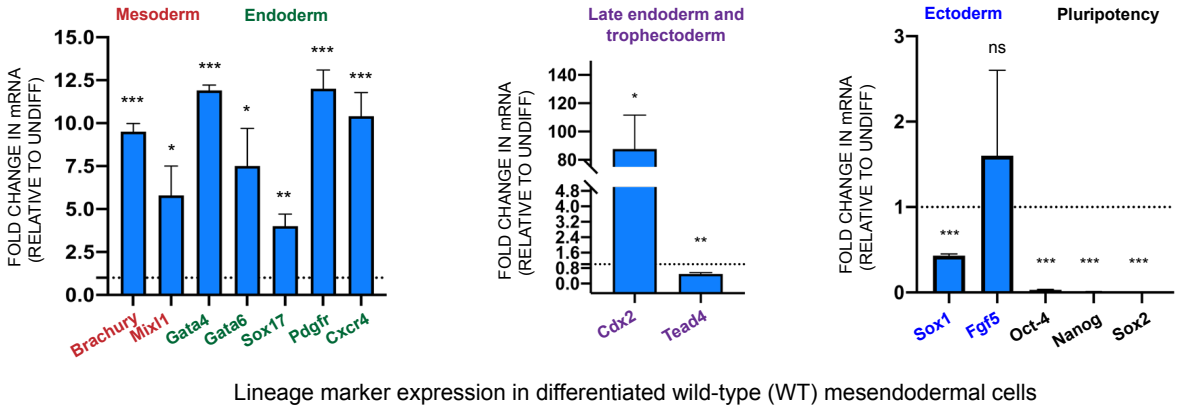

B

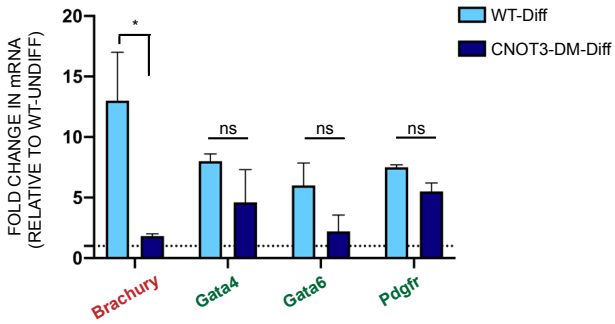

C

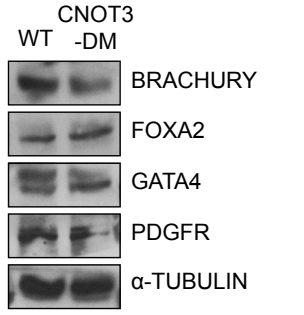

Figure 5: Expression analysis of lineage markers in differentiating *Cnot3*-DM ME cells. A. Analysis of mRNA levels from lineage marker genes after BMP4+FGF2 induced differentiation of wild-type ESCs for 4 days. Values for the undifferentiated (undiff) ESCs were set at 1 as indicated by a horizontal line in each histogram. *Cdx2* is a marker for late endoderm and trophectoderm. *Tead4* is a marker for early trophectoderm. Mean ± SEM; *n*=3. P values in (A) and (B) calculated by unpaired *t*-test, *P<0.05, **P<0.01, ***P<0.001, ns = non significant. **B.** Analysis of mRNA levels of ME markers after BMP4+FGF2 induced differentiation of wild-type (WT) and *Cnot3*-DM ESCs for 4 days. The fold change

is relative to the mRNA level in the undifferentiated WT ESCs set at 1 as indicated by the horizontal line. Error bars represent the mean ± SEM; *n*=2.

C. Representative immunoblot analysis of the protein levels for the indicated lineage markers after BMP4 + FGF2 induced ME differentiation of WT and *Cnot3*-DM ESCs carried out for 4 days. α-Tubulin was used as a loading control.

FIGURE 6

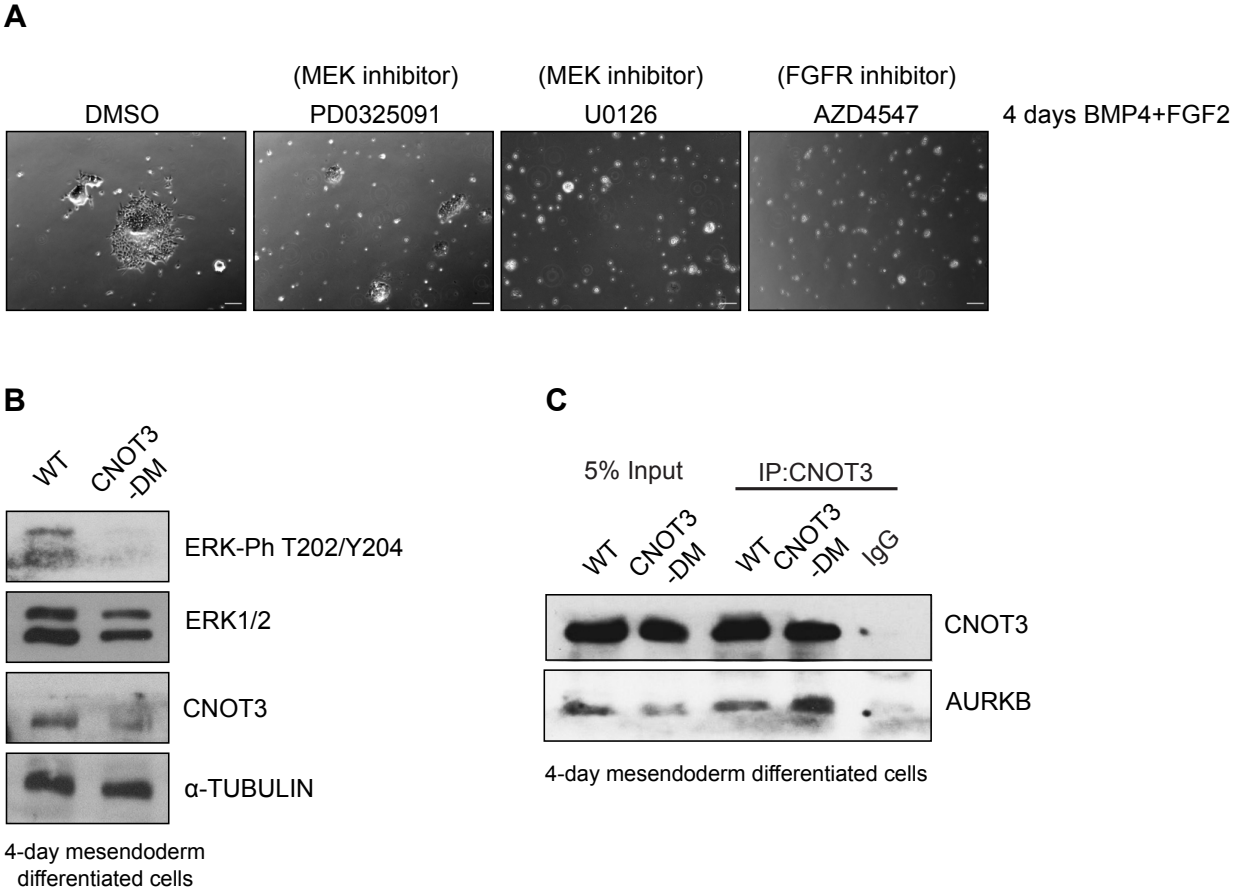

Figure 6: The CNOT3 double mutation reduces ERK phosphorylation during ME differentiation. **A**. Phase-contrast images showing the effects of MEK inhibitors (PD0325091 and U0126), which abolish ERK activity, and the FGFR inhibitor AZD4547, on BMP4 + FGF2 induced ME differentiation of wild-type (WT) ESCs. Differentiations were carried out for 4 days. Each inhibitor was added after two days of differentiation. Vehicle = DMSO. Scale bar = 100 μm. **B**. Representative immunoblot analysis of the indicated proteins carried out on cell extracts from WT and *Cnot3*-DM ESCs subjected to 4 days of BMP4 + FGF2 induced differentiation into ME. Loading control: α-Tubulin. **C**. Co-IP was carried

out with anti-CNOT3 antibody on cell extracts prepared from WT and *Cnot3*-DM ESCs differentiated as in (B). Co-immunoprecipitated proteins were immunoblotted and probed with anti-CNOT3 and anti-Auorora B. Negative control: rabbit IgG. Input = 5% of extracts.

FIGURE 7

A

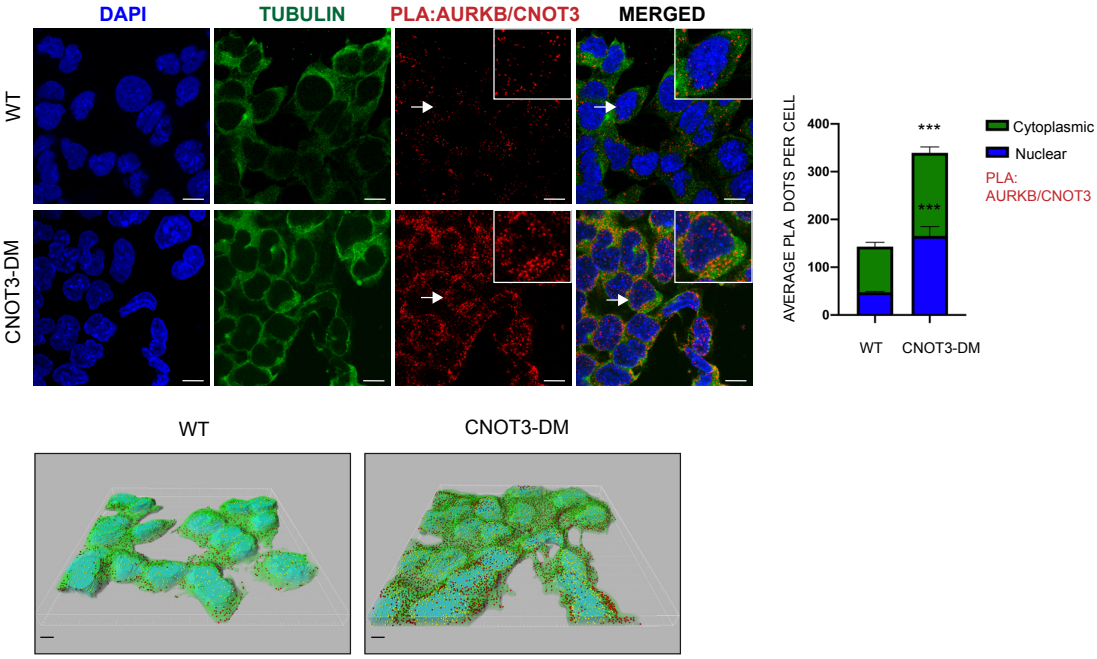
DAPI
TUBULIN
PLA:AURKB/CNOT3
MERGED
WT
CNOT3-DM
AVERAGE PLA DOTS PER CELL
400
300
200
100
0
***
***
Cytoplasmic
Nuclear
PLA:
AURKB/CNOT3
WT
CNOT3-DM
WT
CNOT3-DM

B

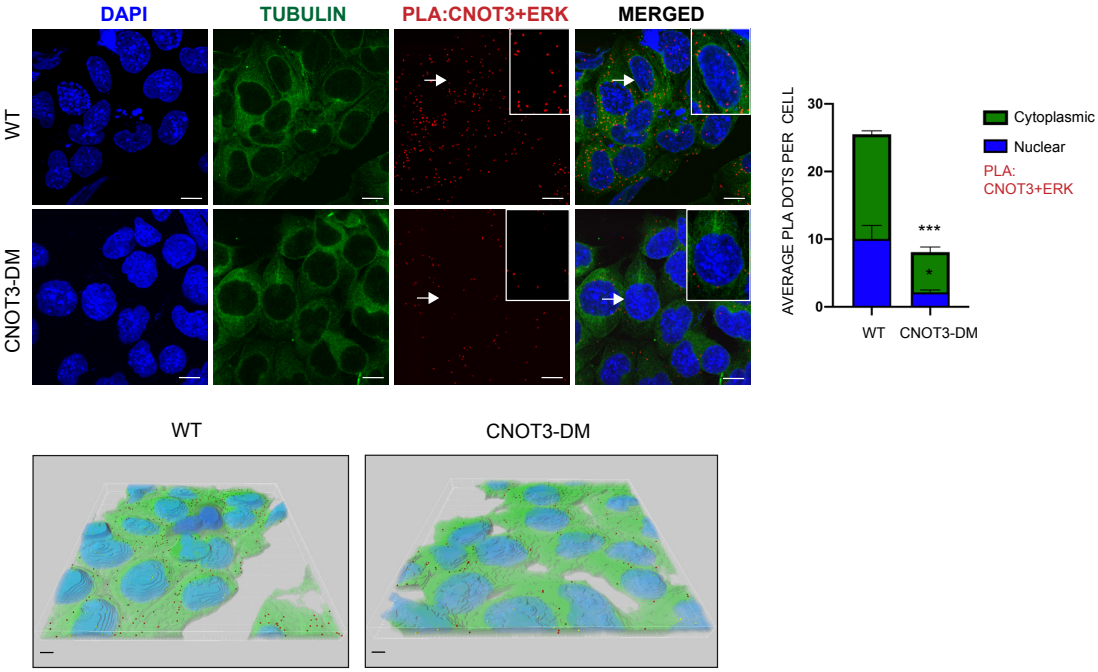
DAPI
TUBULIN
PLA:CNOT3+ERK
MERGED
WT
CNOT3-DM
AVERAGE PLA DOTS PER CELL
30
20
10
0
***
*
Cytoplasmic
Nuclear
PLA:
CNOT3+ERK
WT
CNOT3-DM
WT
CNOT3-DM

C

Cnot3 Δ651-751
Cnot3 Δ701-751
Cnot3 Δ651-700
N-terminal
C-terminal
Coiled Coil
IDR
NAR
CS
NOT box
CNOT3
1
241
605
654
751
10% INPUT
GST
ERK
35S CNOT3
WT
Δ651-700
Δ701-751
Δ651-751
GST PULLDOWN
NORMALISED 35S CNOT3
LEVELS
3.0
2.5
2.0
1.5
1.0
0.5
0.0
*
**
***
WT
Δ651-700
Δ701-751
Δ651-751

Figure 7: Phosphorylation of CNOT3 alters its interaction with Aurora B and ERK in ME cells. A. and **B.** PLA was used to detect interaction between endogenous Aurora B (AURKB) and CNOT3 (A) and CNOT3 and ERK (B) after 4 days of BMP4 + FGF2 induced differentiation of ME cells from wild-type (WT) and *Cnot3*-DM ESCs. Top panels: Red dots represent positive PLA signals. Nuclei were stained with DAPI and cytoplasm with anti-tubulin. Boxed areas show an enlarged image of a cell (indicated by the arrows) from each merged panel. scale bars =10 μm. Bottom panels: Three-dimensional images of the cells were digitally reconstructed, showing the distribution of PLA dots in the nucleus (yellow) and cytoplasm (red) (See Methods). scale bars = 5 μm.. PLA dots were quantified from randomly chosen fields from at least 50 cells for each biological replicate. Histograms represent average number of interactions per cell (dots/cell) in the nucleus (blue) and cytoplasm (green). Mean ± SEM; unpaired *t*-test ***P<0.001 (A) *n*=3 (B) *n*=2. Single antibody controls and PLA of CNOT3 and ERK using a second set of antibodies are shown in Figure S7. **C.** *In vitro* GST pulldown assay using GST-ERK1 and *in vitro* transcribed/translated wild-type (WT) CNOT3 and CNOT3 deletion mutants labelled with ^{35}S-methionine. Left panel: Schematic representation of the deletion mutants of *Cnot3*. Middle panel: Representative *in vitro* GST pulldown assay of GST-ERK1 and ^{35}S-labelled WT CNOT3 and CNOT3 deletion mutants. GST-only was used as a negative control for each pulldown. Input =10% of the respective labelled proteins. Right panel: histogram shows quantification of the band intensities normalized to input and relative to WT CNOT3. Mean ± SEM; *n*=3 (unpaired *t*-test *P<0.05, **P<0.01, ***P<0.001).

FIGURE 8

A

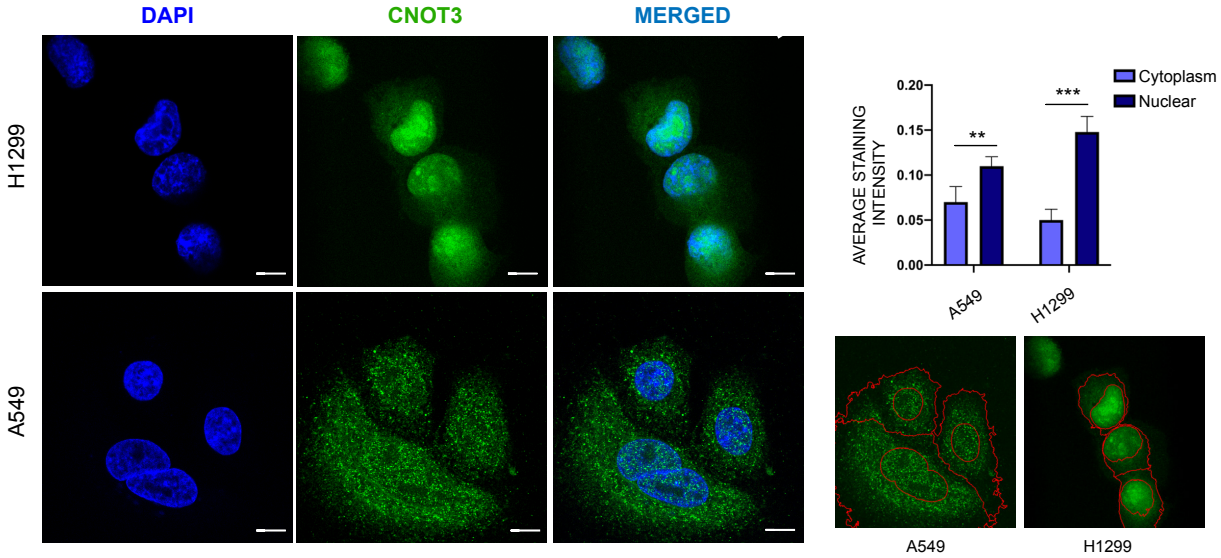

B

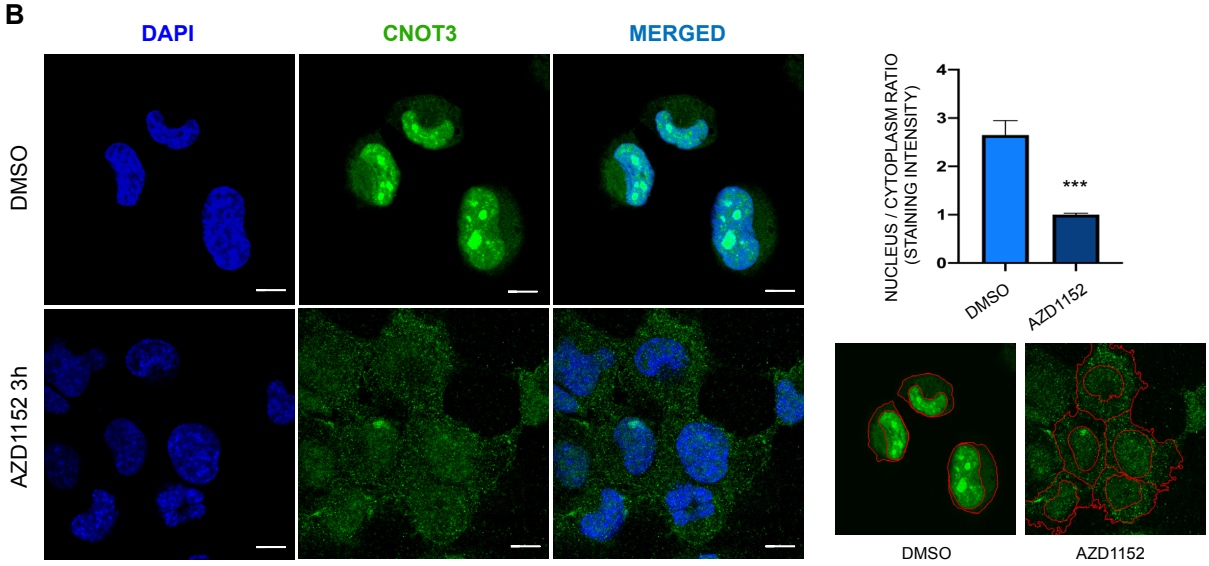

H1299 cells

C

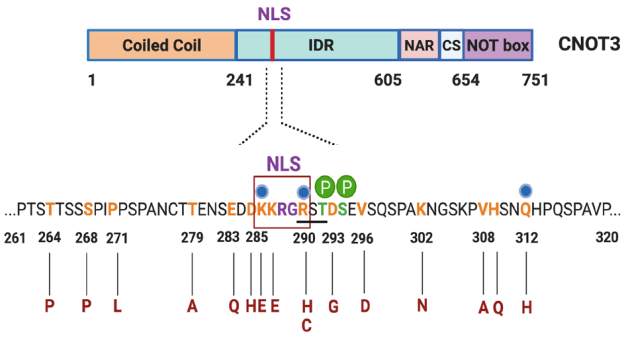

Mutation	Number of patients	Tissue
T264P	1	Thyroid
S268P	1	Upper aerodigestive tract
P271L	1	Lung
T279A	1	Ovary
E283Q	1	Urinary tract
D285H	1	Breast
K286E ●	4	Colon
K287E	1	Colon
R290C ●	2	Colon
R290H ●	2	Lung, Colorectal
D293G	1	Lung
V296D	1	Colon
K302N	1	Endometrium
V308A	1	Liver
H309Q	1	Liver
Q312H ●	2	Liver

NLS

● mutations observed in multiple patients

Figure 8: Phosphorylation by Aurora B promotes nuclear localisation of CNOT3 in a metastatic NSCLC cell line

A. Comparison of nuclear and cytoplasmic localisation of CNOT3 in two NSCLC cell lines. The H1299 line was derived from a lymph node metastasis and the A549 line from a lung adenoma. Left panel: H1299 cells (top) and A549 cells (bottom) immunostained with anti-CNOT3 and counterstained with DAPI (scale bar: 10 μm). Right panel: Histogram shows digital quantification of the average intensities of the nuclear and cytoplasmic staining for CNOT3 in the H1299 and A549 cells. Mean ± SEM; *n*=3 (unpaired *t*-test **P<0.01, ***P<0.001). Images (bottom) show representative fields depicting segmentation of the cells and of the nuclei used for the quantification. Quantification was performed on at least 30 cells from randomly chosen fields for each biological replicate. **B.** Effect of the Aurora B inhibitor AZD1152 on nuclear and cytoplasmic localization of CNOT3 in H1299 cells. Left panel panel: H1299 cells were incubated for 3 hours with AZD1152 (bottom) or with vehicle (DMSO, top) and were then immunostained as in (A) (scale bar = 10 μm). Right panel: Histogram shows quantification of the average ratio of nuclear to cytoplasmic staining for CNOT3 in the AZD1152 and vehicle-treated cells. Mean ± SEM; *n*=3 (unpaired *t*-test ***P<0.001). Images (bottom) show representative fields as in (A). Quantification was performed on at least 30 cells from randomly chosen fields for each biological replicate.

C. Missense mutations described in human cancer patients in the region of CNOT3 spanning residues 261 to 320. Blue spheres indicate mutations that have been observed in more than one patient. The nuclear localisation signal (NLS) is indicated by red rectangles in the left and right panels and the Aurora B consensus is underlined in the left panel. P = phosphorylation sites

FIGURE 9

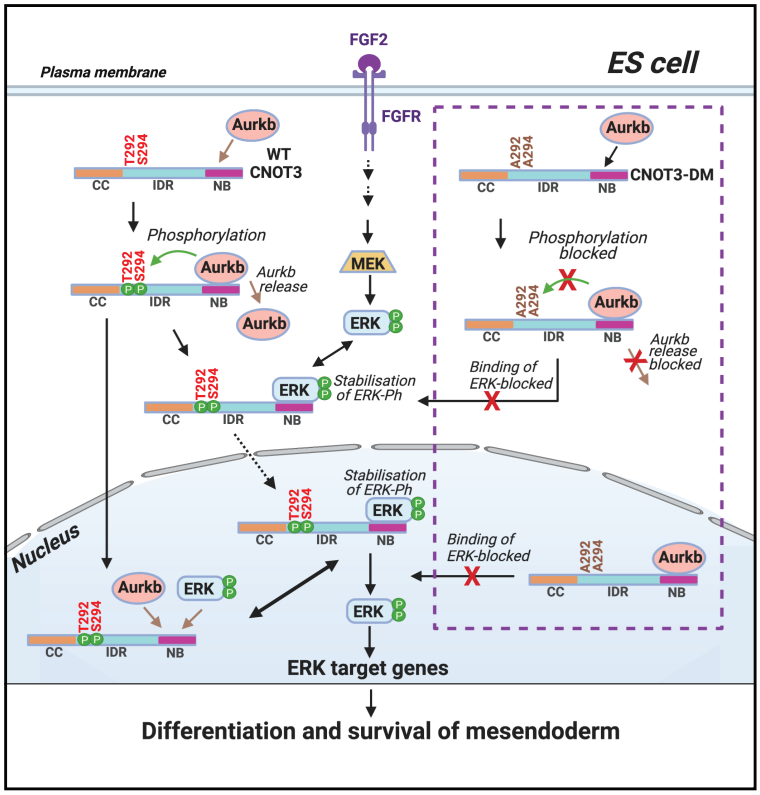

Figure 9. Schematic model showing the proposed regulation of ERK activity by Aurora B and CNOT3. Aurora B (AURKB) binds to the NOT box (NB) of CNOT3 (for clarity the additional synergistic contact with the amino-terminal coiled-coil (CC) domain is not shown). The bound Aurora B phosphorylates CNOT3-T292/S294, located adjacent to a nuclear localization signal in the intrinsically disordered region (IDR) of CNOT3 and promotes uptake of CNOT3 into the nucleus. Phosphorylation of CNOT3 also causes bound Aurora B to be released, allowing phospho-ERK (ERK-Ph) to bind to the NOT box. This results in stabilisation of ERK-Ph in the cytoplasm and nucleus and may also facilitate transport of ERK-Ph into the nucleus. Mutation of CNOT3-T292/S294 to A (CNOT3-DM) prevents phosphorylation of these residues by Aurora B (depicted inside the dashed box). This blocks release of Aurora B and prevents binding of ERK to the NOT box, resulting in destabilisation and downregulation of ERK-Ph.

Legend to Supplementary Video 1

Time-lapse imaging of BMP4/FGF2-induced differentiation of wild-type and *Cnot3*-DM ESCs. Images were collected at 30 minute intervals from day 3 to day 7 of the differentiation (see Methods). Scale-bar = 100 μM.